

# Modeling tensile crack propagation in concrete gravity dams via crack-path-field and strain injection techniques

I. F. Dias<sup>1,a</sup>, J. Oliver<sup>2,3,b</sup>, J. V. Lemos<sup>1,c</sup> and O. Lloberas-Valls<sup>3,d</sup>

<sup>1</sup>Laboratório Nacional de Engenharia Civil (LNEC)  
Avenida Brasil 101,1700 Lisboa, Portugal

<sup>2</sup>E.T.S. d'Enginyers de Camins, Canals i Ports, Technical University of Catalonia

<sup>3</sup>CIMNE - Centre Internacional de Metodes Numerics en Enginyeria

Campus Nord UPC, Edifici C-1, c/Jordi Girona 1-3, 08034 Barcelona, Spain

<sup>a</sup>idias@lnec.pt, <sup>b</sup>xavier.oliver@upc.edu, <sup>c</sup>vlemos@lnec.pt, <sup>d</sup>olloberas@cimne.upc.edu

**Keywords:** concrete gravity dams, fracture, computational material failure, strong discontinuities, crack-path field, strain injection, mixed formulation

**Abstract:** This work investigates tensile crack propagation in concrete gravity dams by using some recently developed numerical techniques (crack-path field and strain injection techniques) [1-3]. The work carefully addresses aspects related to mesh independence, robustness and computational cost, which are the main issues in fracture modeling. The novel technique consists of a procedure to insert, in the selected domain areas, specific strain fields for enhancing the performance of the underlying finite elements in modeling fracture. Representative numerical simulations of concrete dams show the accuracy and robustness of the methodology. The code used for the simulations is open-source and available at <http://www.cimne.com/compdesmat/>.

## 1 Introduction

Nowadays, structural safety of large dams remains a great concern due to the high potential risk associated to this kind of structures. A dam failure, followed by a sudden flood wave, can result in large life losses and in strong environmental and economic impacts, as it was reported for several catastrophic failure cases [5, 6]. Historically, the main causes of significant dam failures are related to foundation defects (erosion, sliding on its rock foundation, *etc.*) [7-9]. Structural failures, when not directly caused by foundation movements, are less frequent but its importance should not be minimized in the design neither in the safety control of the dam. Due to the importance of these structures, it is a worldwide standard practice to monitor continually dams as a part of the safety control process [10], which supports afterwards the safety assessment and decision. On the other hand, quantifying realistically concrete dams' safety factors is a complex engineering question that depends on multiple phenomena affecting the performance and resistance of the dam and its foundation.

In this work attention is focused on crack propagation through the dam body. Cracks progressing deep inside gravity dams can seriously affect its structural safety. Computational failure analysis can be an effective tool for realistically predict the eventual crack profiles and the ultimate structural resistance, allowing improved estimation of the structural safety factor.

The importance of computational methods in assessing dams safety and damage was soon recognized by some authors in the 1980s, which have used *linear elastic fracture mechanics* [11-15] to perform the first computational simulations of fracture in concrete dams. These authors argued that, due to the large size of dams, the fracture process zone is small in front of the overall structure and therefore *linear elastic fracture mechanics* can be applicable with limited errors, since failure occurs in a brittle (or quasi-brittle) manner. On the other hand, other authors argue that, due to the specific characteristics of dam concrete (that can have characteristic length up to 10 times greater than common concrete), the non-linear effects should not be neglected, even for large dams [16, 17].

Apart from this theoretical and important question, in the 1990s, nonlinear fracture analysis starts becoming further used in fracture modeling of concrete dams. Depending on the manner that the decohesion process at the crack interface is modeled, two major descriptions were used:

1. In the *cohesive* (or discrete) *approach* [18, 19] the non-linear mechanical behavior is described by introducing a traction separation law (relating the traction vector and the vector of displacement jump) along the surface where the decohesive process occurs (typically coincident with the element sides).
2. In the *continuum approach* [20-23] the non-linear mechanical behavior at the interface is described by a standard stress-strain constitutive equipped with softening, to account for the stress release associated to failure. Here the main assumption consists in admitting that the displacement jump can be captured in a *smear*ed manner throughout the localization band.

In both approaches fracture energy plays a fundamental role in order to make results physically meaningful (ensuring correct energy dissipation and overcoming the mesh size dependence). The main flaw of the initial methods based on these approaches was the spurious dependence on the mesh alignment, which is critical because different meshes can deliver different results, in terms either of the crack trajectory or of the dissipated energy. The main consequences of mesh dependence phenomena are well documented in the literature, and consist, essentially, in two types of undesirable behavior:

- *Mesh bias dependence*: Refers to the spurious tendency of the crack to follow certain preferred directions related to the mesh alignment, *i.e.* the crack tends to propagate parallelly to the element sides avoiding zigzagging. The main inconvenience of this dependence is that it can lead to unrealistic/unphysical failure mechanisms, with consequences also in the ultimate structural load carrying capacity, which may be over or under-estimated.
- *Stress locking effects*: Refers to the lack of ability of finite elements to capture strain localization, in a one-element-width localization band, without spurious stress transfer to the neighboring elements. The principal inconvenient of stress locking is the extra dissipation that occurs in elements outside the localization band which results in an over-stiffer behavior that leads to an overestimation of the ultimate structural load carrying capacity, which is not on the safety side.

Despite these limitations, which make re-meshing techniques mandatory to obtain mesh independent results, interesting applications to concrete dams have been reported in the literature by using both *cohesive* [4, 24, 25] and *continuum models*. The fact that the continuum approach can be implemented in a standard non-linear finite element code by just introducing strain softening in the constitutive

model, made the approach widely used and various constitutive models were explored for modeling crack propagation in concrete dams. For example in [17, 26] applications by using *smear crack models* are reported and in [27-30] the authors have applied *damage/plasticity based models*.

In the 1990s, aiming to overcome the flaws of the classical methods, new developments and enhancements have been proposed in the context of the continuum models. Depending on how the crack/slip-line (displacement jump) is captured by the numerical methods, the continuum approaches can be classified in three groups:

- The *strain-localization-based methods*, in which, due to strain softening, strains tend naturally to localize in narrow bands that under ideal conditions encompass just one finite element. This approach corresponds to the aforementioned, firstly proposed, continuum models. These are the most conceptually simple and intuitive models for simulating crack propagation<sup>1</sup> but are known to suffer from mesh bias dependence and stress locking flaws.
- In the *supra-element-band methods*, a regularized displacement jump is captured by a band of finite elements encompassing several elements across it. The bandwidth is then considered a characteristic length. This class of models include material-regularization-based approaches (non-local, gradient or Cosserat models [31, 32] and the, more recent, phase field models for fracture [33]). In general, good results are obtained, although the fact that the size of the finite element is smaller than the, very tiny, characteristic length implies that a huge number of elements are required, this leading to large computational costs.
- In the *intra-elemental methods*, the discontinuity interface settles inside the finite element, thus, no restrictions in the size of the finite elements exist and very coarse meshes can be used. In these methods, the finite elements are enriched with additional discontinuous displacement modes and are termed E-FEM or X-FEM if the support of the additional modes is elemental or nodal based, respectively. The performances of both methods are similar [34], but some computational benefits from the E-FEM side can be obtained due to the elemental support of the enriching modes that can be condensed out, this leading to a lower computational cost.

However, in both methods, robustness depends on the precise determination of the position of the discontinuity and this, is classically done by means of *crack-tracking algorithms* that are cumbersome to implement, have a code-invasive character and may seriously affect the robustness of the method [35]. These drawbacks seem to be responsible for its little use in modeling real-life problems and in commercial codes incorporation.

Outside the finite element framework, alternative methodologies, of diverse natures, have been also proposed for material failure modeling:

- In the *discrete element methods* [36, 37] the idea of continuum media is left aside being formulated in terms of rigid discrete elements that interact with each other according to contact laws. For modeling fracture in structures without “a-priori” preferable failure

---

<sup>1</sup> These classical models do not require any enhancement more than a proper regularization of the softening modulus for ensuring a correct dissipation of energy.

surfaces, the discrete elements are generally chosen to be circular or spherical particles and the corresponding inter-particle contacts can either be assumed as brittle or following a given softening curve [38, 39]. These methods model directly the meso-structure of the materials being therefore computationally more demanding than the continuum models (that are at the macro-scale level).

- The *lattice* models have been initially developed to deal with random heterogeneous materials [40]. The structure is discretized as a lattice composed of Bernoulli beams that transfer normal forces, shear forces and bending moments. Usually linear elastic analyses are performed and beam elements that exceed tensile strength are removed [41, 42], and consequently, their inertial effects are neglected.
- *Multi-scale* approaches with different theoretical background have been proposed (see [43] for a general insight). Usually, in these approaches two distinct length scales are considered: one corresponding to the structural size (macro scale) and other corresponding to the zone, near the crack tip, where the fracture is being processed, which intends to capture the complex phenomena of fracture deriving from the material micro-structure (*e.g.* the atomistic simulations of [44]).

In the last two decades, some of the previous mentioned E-FEM and X-FEM methods, material-regularization-based approaches, phase field models, discrete/lattice and multi-scale approaches have attracted large interest of the computational mechanics community, and a huge number of papers have been published in the different fields of research. However, so far, applications were mostly restricted to academic benchmarks and few cases of real-life structures have been reported [45]. For this reason, these methods are not regarded, yet, as a true reliable alternative for modeling crack propagation in concrete dams, such that can help in the design or in the safety control of these large structures. Some flaws of these methods that make general authors to be reluctant in using them are the following:

- Higher computational cost relatively to the more classical methods, with consequences in the computational times and, thus, in productivity.
- Increasing theoretical complexity, which makes the new methodologies less appealing for more “practical” developers and general engineers.
- Difficulties of implementation in standard non-linear finite element codes. In some cases, the intrusive character of the formulations, make the methodologies quite cumbersome to implement. This can be a dissuasive factor for new implementers and developers.
- Unavailability of commercial or open-source software. Most of these new numerical techniques have not been yet incorporated to commercial codes. The insufficient interest of commercial companies can be related with the three flaws enumerated previously. Regarding to the lack of open-source software, usually, in the computational failure mechanics field, the developing authors do not distribute their computational codes in open source formats or, if so, the code is not properly publicized (for example in the corresponding paper).

## 1.1 Objectives and main assumptions of the work

In this work, the departure point are the recently developed crack-path-field and strain-injection techniques [1-3, 46], that have proved to be a valuable tool for capturing propagating material failure in a set of 2D “quasi-static” academic benchmarks. The main novelty of this method is the

introduction of the strain injection concept, *i.e.* the imposition of goal-oriented strain-fields, in selected areas of the domain and at specific stages, to improve the performance of the resulting model in capturing propagating material failure.

In fact, a proper combination of these techniques (crack-path field and strain injection) and a stabilized mixed formulation leads to a general mesh independent methodology ready for failure modeling of real-life large concrete structures, like concrete dams. The methodology provides the classical advantages (mesh independence and low computational cost) of the *intra-elemental* methods while being minimally intrusive for the simulation code in which it is implemented. These interesting properties allow us to think that the new techniques show a strong potential to be competitive in front of other promising approaches aiming at capturing propagating cracks (the phase-field models [47], the full mixed approach<sup>2</sup> of [48] and the recent improvements to the strong discontinuity approach either in the E-FEM or X-FEM versions [49-51], *etc.*).

So far, the methodology was implemented only for 2D cases, with applications limited to isothermal quasi-static problems. The kinematical description of the motion is also simplified to infinitesimal strains. The authors are aware that seismic analyses, in which inertial effects cannot be neglected, are one of the main actual concerns in terms of dam structural safety and, therefore, it will be considered in subsequent work. Notice that by neglecting the inertial effects, more realistic comparisons with experimental results can be performed since physical phenomena difficult to quantify and measure, like the damping mechanisms, play no role. In quasi-static cases, the necessary physical parameters to introduce in the model are limited to the elastic constants (Young's modulus and Poisson's ratio), the ultimate tensile strength and the material fracture energy, which can be measured in laboratory. Moreover, the interior fluid pressure in the open cracks was also neglected. Although the authors are well aware of the importance of this issue (hydraulic fracture), this is not in the scope of this work, which is essentially devoted to evaluate the benefits of the proposed computational methods for modeling crack propagation in dams.

The main objective of the present paper is to assess the capabilities of the new numerical tools, so far with applications limited to some academic benchmarks, in modeling tensile crack propagation in concrete dams. The theoretical summary of the methodology presented in sections 2, 3 and 4, has the exclusive goal of providing the reader with the general ideas about the method and it does not pretend to be exhaustive. In [1] a deeper presentation of the formulation and its implementation details can be consulted by the interested readers.

The numerical simulations, in section 5, show the potential of the methodology to model fracture propagation in concrete dams. Aspects related to mesh independence (mesh bias and stress locking), robustness, and computational cost, which are the main issues in material failure modeling, are carefully addressed.

---

<sup>2</sup> This mixed approach uses continuous interpolations both for the displacements and the strains. The computational cost is higher due to the increased number of degrees of freedom per node: from 2 (displacements) to 5 (2 displacements plus 3 strains) in 2D cases.

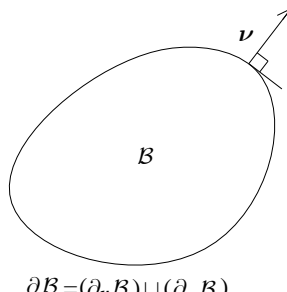
## 2 Finite element setting. Variational approaches to the mechanical problem

### 2.1 Displacement based finite element formulation

Standard finite element formulations of the non-linear mechanical problem (summarized in Box 1) are usually displacement-based, in the sense that the displacement field,  $\mathbf{u}$ , is the independent unknown to be interpolated by using some suitable interpolation functions. The strains,  $\boldsymbol{\varepsilon}$ , are computed from the compatibility equation, (3), and the stresses,  $\boldsymbol{\sigma}$ , via the constitutive relation, (4). The one field variational equation corresponding to the equilibrium equation of the mechanical problem in Box 1 reads (in rate form):

$$\int_B \nabla^s \boldsymbol{\eta} : \dot{\boldsymbol{\Sigma}} \nabla^s \dot{\mathbf{u}} \, dB - \dot{W}^{ext}(\boldsymbol{\eta}, \dot{\mathbf{b}}, \dot{\mathbf{t}}^*) = 0, \quad \forall \boldsymbol{\eta}. \quad (1)$$

Equation (1) is equivalent to the classic virtual work principle where  $\dot{W}^{ext}(\boldsymbol{\eta}, \dot{\mathbf{b}}, \dot{\mathbf{t}}^*)$  stands for the work produced by the external forces and  $\boldsymbol{\eta}$  for the test function.

Given the external actions, $\dot{\mathbf{u}}^*(\mathbf{x}, t)$ , $\dot{\mathbf{t}}^*(\mathbf{x}, t)$ and $\dot{\mathbf{b}}(\mathbf{x}, t)$ , find $\dot{\mathbf{u}}(\mathbf{x}, t)$ , $\dot{\boldsymbol{\varepsilon}}(\mathbf{x}, t)$ and $\dot{\boldsymbol{\sigma}}(\mathbf{x}, t)$ :		
 <p style="text-align: center;"><math>\partial B = (\partial_u B) \cup (\partial_\sigma B)</math></p>	$\nabla \cdot \dot{\boldsymbol{\sigma}} + \dot{\mathbf{b}} = 0$ $\dot{\boldsymbol{\varepsilon}} = \nabla^s \dot{\mathbf{u}}$ $\dot{\boldsymbol{\sigma}} = \dot{\boldsymbol{\Sigma}}(\dot{\boldsymbol{\varepsilon}})$ $\left. \begin{aligned} \dot{\mathbf{u}} &= \dot{\mathbf{u}}^*(\mathbf{x}, t), \quad \forall \mathbf{x} \in \partial_u B \\ \dot{\boldsymbol{\sigma}} \cdot \boldsymbol{\nu} &= \dot{\mathbf{t}}^*(\mathbf{x}, t), \quad \forall \mathbf{x} \in \partial_\sigma B \end{aligned} \right\}$	<p>Equilibrium equation (2)</p> <p>Compatibility equation (3)</p> <p>Constitutive equation (4)</p> <p>Boundary conditions (5)</p>

Box 1 Mechanical problem in body  $B$ , where  $\partial_u B$  and  $\partial_\sigma B$  are the portions of the boundary,  $\partial B$ , where Dirichlet and Newman conditions are defined,  $\boldsymbol{\nu}$  is its outward normal and  $\dot{\mathbf{u}}^*(\mathbf{x}, t)$ ,  $\dot{\mathbf{t}}^*(\mathbf{x}, t)$  and  $\dot{\mathbf{b}}(\mathbf{x}, t)$  are the prescribed displacements, tractions and body loads, respectively.

In the context of material failure modeling, it is well known that displacement based finite element formulations are not adequate for modeling highly concentrated strain localization processes as the ones that occur in the onset of crack initiation and propagation.

### 2.2 Mixed $\mathbf{u}/\boldsymbol{\varepsilon}$ formulation

An alternative approach is the one based on two fields: displacements and strains,  $\mathbf{u}/\boldsymbol{\varepsilon}$ , in which both, the equilibrium (2) and the compatibility equation (3) are weakly enforced:

$$\int_B \nabla^s \boldsymbol{\eta} : \dot{\boldsymbol{\Sigma}}(\dot{\boldsymbol{\varepsilon}}) \, dB - \dot{W}^{ext}(\boldsymbol{\eta}, \dot{\mathbf{b}}, \dot{\mathbf{t}}^*) = 0, \quad \forall \boldsymbol{\eta}, \quad (a)$$

$$\int_B \boldsymbol{\mu} : \dot{\boldsymbol{\varepsilon}} - \nabla^s \dot{\mathbf{u}} \, dB = 0, \quad \forall \boldsymbol{\mu}. \quad (b)$$

In contrast with the one-field approach in equation (1), the two field format in equation (6) opens a number of additional possibilities for modeling material failure. The problem can be inserted in the context of the assumed strain methods [52], this providing additional freedom in the choice of the strains that can lead to formulations with enhanced kinematics and flexibility, which might be valuable for material failure modeling.

By choosing standard bi-linear interpolation functions for the displacement field and element-wise constant strains in four-noded quadrilateral finite elements, the finite element approximation of equation (6) reads:

$$\begin{aligned} \sum_{e=1}^{n_{elem}} \int_{\mathcal{B}^{(e)}} \nabla^s \boldsymbol{\eta}^h(\mathbf{x}) : \dot{\boldsymbol{\Sigma}}(\dot{\boldsymbol{\varepsilon}}^{(e)}) d\mathcal{B} &= \dot{W}^{ext}(\boldsymbol{\eta}^h, \dot{\mathbf{b}}, \dot{\mathbf{t}}^*) \quad , \quad \forall \boldsymbol{\eta}^h, \quad a) \\ \int_{\mathcal{B}^{(e)}} \boldsymbol{\mu}^{(e)} (\dot{\boldsymbol{\varepsilon}}^{(e)} - \nabla^s \dot{\mathbf{u}}^h(\mathbf{x})) d\mathcal{B} &= 0 \quad \forall \mathcal{B}^{(e)} \subset \mathcal{B}^h, \quad \forall \boldsymbol{\mu}^e. \quad b) \end{aligned} \quad (7)$$

Taking the test function,  $\boldsymbol{\mu}^{(e)}$ , and the discretized strains,  $\dot{\boldsymbol{\varepsilon}}^{(e)}$ , in equation (7), as element-wise constant in the element,  $\mathcal{B}^{(e)}$ , equation (7-b) can be trivially solved, at the element level, as:

$$\dot{\boldsymbol{\varepsilon}}^{(e)} = \frac{\int_{\mathcal{B}^{(e)}} \nabla^s \dot{\mathbf{u}}^h(\mathbf{x}) d\mathcal{B}}{meas(\mathcal{B}^{(e)})} = \overline{\nabla^s \dot{\mathbf{u}}^h}^{(e)} \quad , \quad e = 1, \dots, n_{elem}. \quad (8)$$

Where notation  $\overline{(\cdot)}^{(e)}$  stands for the spatial average of  $(\cdot)$  on the element  $(e)$  and  $meas(\cdot)$  for the area of  $(\cdot)$ . Inserting equation (8) into equation (7-a) yields,

$$\sum_{e=1}^{n_{elem}} \int_{\mathcal{B}^{(e)}} \nabla^s \boldsymbol{\eta}^h(\mathbf{x}) : \dot{\boldsymbol{\Sigma}}(\overline{\nabla^s \dot{\mathbf{u}}^h}^{(e)}) d\mathcal{B} = \dot{W}^{ext}(\boldsymbol{\eta}^h, \dot{\mathbf{b}}, \dot{\mathbf{t}}^*) \quad , \quad \forall \boldsymbol{\eta}^h. \quad (9)$$

REMARK 2-1 It can be shown the equivalence of the mixed  $\mathbf{u}1 / \varepsilon 0$  formulation for quadrilateral elements in equation (9) with the reduced integration of displacement based formulation [1-3, 53], which is known to be unstable when applied to the whole domain  $\mathcal{B}$ . In practice the instability is noticeable by the spurious propagation of zero energy (hourglass) displacement modes that become dominant and pollute the solution in terms of the displacement field.

### 2.3 Stabilized mixed $\mathbf{u}1 / \varepsilon 0$ formulation

In the past, to overcome the instability originated by reduced integration methods, diverse stabilization procedures and hourglass control techniques, with different theoretical foundations, have been proposed. [54, 55]. Here we use the stabilization term proposed in [1-3]<sup>3</sup>:

$$\dot{W}^{stab^{(e)}} = \tau^{(e)}(t) \int_{\mathcal{B}^{(e)}} \nabla^s \boldsymbol{\eta}^h(\mathbf{x}) : [\dot{\boldsymbol{\Sigma}}(\dot{\boldsymbol{\varepsilon}}^{(e)}) - \dot{\boldsymbol{\Sigma}}(\nabla^s \dot{\mathbf{u}}^h(\mathbf{x}))] d\mathcal{B}. \quad (10)$$

Where  $\tau^{(e)}(t) \in [0,1]$  is a stabilization parameter, which, can be specific for every element and evolve along time. Adding the stabilization term (10) to equation (9) and rearranging terms we get:

---

<sup>3</sup> The proposed stabilization term in equation (10) falls into the family of consistently stabilized methods (see [56, 57]). The consistency of the stabilization stems from equation (7-b), which implies that with mesh refinement  $\dot{\boldsymbol{\varepsilon}}^{(e)} \rightarrow \nabla^s \dot{\mathbf{u}}^h$ , this meaning that the stabilization term in (10) vanish with mesh refinement regardless of the value of the stabilization parameter.

$$\begin{aligned}
& \sum_{e=1}^{n_{elem}} \tau^{(e)}(t) \underbrace{\int_{\mathcal{B}^{(e)}} \nabla^s \boldsymbol{\eta}^h : \dot{\boldsymbol{\Sigma}}(\nabla^s \dot{\mathbf{u}}^h(\mathbf{x})) d\mathcal{B}}_{\substack{\text{full integration} \\ \text{(irreducible) form}}} + \\
& + \sum_{e=1}^{n_{elem}} (1 - \tau^{(e)}(t)) \underbrace{\int_{\mathcal{B}^{(e)}} \overline{\nabla^s \boldsymbol{\eta}^h}^{(e)} : \dot{\boldsymbol{\Sigma}}(\overline{\nabla^s \dot{\mathbf{u}}^h}^{(e)}) d\mathcal{B}}_{\substack{\text{reduced integration} \\ \text{(mixed) form}}} = \dot{W}^{ext}(\boldsymbol{\eta}^h, \dot{\mathbf{b}}, \dot{\mathbf{t}}^*), \quad \forall \boldsymbol{\eta}^h.
\end{aligned} \tag{11}$$

The stabilized mixed formulation in equation (11) can be regarded as a weighted combination of the irreducible displacement based formulation (fully integrated term) and the mixed displacement-strain formulation (reduced integrated term), weighted by  $\tau^{(e)}$  and  $(1 - \tau^{(e)})$  respectively.

After some straightforward manipulations, equations (11) can be rearranged, in a more suitable form for implementation purposes, as:

$$\begin{aligned}
& \sum_{e=1}^{n_{elem}} \int_{\mathcal{B}^{(e)}} \nabla^s \boldsymbol{\eta}^h : \dot{\boldsymbol{\sigma}}^{(e)}(\mathbf{x}) d\mathcal{B} = \dot{W}^{ext}(\boldsymbol{\eta}^h, \dot{\mathbf{b}}, \dot{\mathbf{t}}^*), \quad \forall \boldsymbol{\eta}^h, \\
& \dot{\boldsymbol{\sigma}}^{(e)}(\mathbf{x}) = \tau^{(e)} \dot{\boldsymbol{\Sigma}}(\nabla^s \dot{\mathbf{u}}_i^h(\mathbf{x})) + (1 - \tau^{(e)}) \dot{\boldsymbol{\Sigma}}(\overline{\nabla^s \dot{\mathbf{u}}^h}^{(e)}).
\end{aligned} \tag{12}$$

where  $\dot{\boldsymbol{\sigma}}^{(e)}$  are termed the *stabilized stresses*.

REMARK 2-2 Analyzing expression (12), it is noticeable that, for  $\tau^{(e)} = 1$  the method is equivalent to the standard irreducible formulation, whereas for  $\tau^{(e)} = 0$ , the stabilization term vanishes and the unstable mixed formulation is recovered. In previous works of the authors [1, 3], was found that  $\tau^{(e)} = 0.1$  provides a good balance, since the hourglass instabilities of the pure mixed formulation are avoided while keeping the improved properties of the formulation for strain localization modeling.

REMARK 2-3 The improved properties of the stabilized mixed formulation were shown in [1, 3] and are related to the improved flexibility of the finite elements kinematics, which largely enhance the propagation capabilities of the elements (strongly alleviating mesh bias defects). On the other hand, the kinematics still exhibits a limited capability for describing the mechanical behavior of a crack inside a finite element without spurious stress transfer to the neighboring elements (stress locking phenomena). For this reason some strain injection modes will be applied.

### 3 Strain-injection techniques

*Strain injection* refers to a general numerical technique that consists of inserting, in selected parts of the domain and during different stages of the simulation, specific strain fields, that have the goal of enhancing the performance of the finite elements. The key point of this technique is to split the domain into two disjoint subdomains: the injection domain,  $\mathcal{B}_{inj}$ , where some enhanced strain modes are injected, and the remaining part of the body where the underlying finite element formulation is used (see Figure 1).



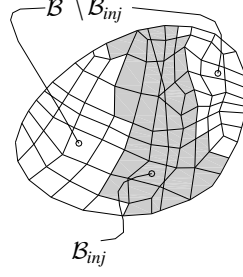


Figure 1 Discretized domain.

### 3.1 Strain-injection techniques and mixed formulations for failure analysis

For modeling tensile crack propagation in concrete gravity dams we propose to use the mixed stabilized finite element formulation<sup>4</sup> (presented in section 2.3), as the underlying formulation, due to its improved performance for modeling strain localization processes. Therefore, considering a finite element discretization and the domain split of Figure 1, the variational equation of the mechanical problem (equivalent to the virtual work principle) can be written as:

$$\underbrace{\int_{\mathcal{B} \setminus \mathcal{B}_{inj}} \nabla^s \boldsymbol{\eta}^h : \dot{\boldsymbol{\sigma}}^{(e)} d\mathcal{B}}_{\text{Stabilized mixed term}} + \underbrace{\sum_{\forall \mathcal{B}^{(e)} \subset \mathcal{B}_{inj}(t)} \int_{\mathcal{B}^{(e)}} \nabla^s \boldsymbol{\eta}^h : \dot{\boldsymbol{\Sigma}}(\dot{\boldsymbol{\varepsilon}}_{inj}^{(e)}) d\mathcal{B}}_{\text{Strain injection term}} = \dot{W}^{ext}(\boldsymbol{\eta}, \dot{\mathbf{b}}, \dot{\mathbf{t}}^*), \quad \forall \boldsymbol{\eta}^h. \quad (13)$$

Where the work produced by the internal forces is computed by the sum of two terms. The first one, the mixed term, corresponds to that part of the domain where the mixed stabilized formulation of equation (12) is used. The second term, the strain injection term, corresponds to that part of the domain where a specific strain field,  $\dot{\boldsymbol{\varepsilon}}_{inj}^{(e)}$ , is injected in the constitutive equation  $\dot{\boldsymbol{\Sigma}} \cdot$  of those elements,  $\mathcal{B}^{(e)}$ , belonging to the injection domain,  $\mathcal{B}_{inj}(t)$ . Here, new equations defining the enhanced strain modes,  $\dot{\boldsymbol{\varepsilon}}_{inj}^{(e)}$ , should be added to the system (see section 3.2.1 and 3.2.2).

### 3.2 Strain-injection modes

In the context of material failure modeling, the injected strain modes have the goal of enhancing the performance of the finite elements in capturing strain localization such that the mechanical behavior of a crack can be captured inside the finite elements without spurious stress locking effects. In [1] two strain fields were proposed to be injected in quadrilateral elements: the constant strain mode and the discontinuous displacement mode.

#### 3.2.1 Constant Strain Mode (CSM) injection

The *constant strain mode injection* consists of assuming constant strains within the finite element. This can be formalized by using the displacement-constant strain mixed formulation ( $\mathbf{u}1 / \varepsilon_{inj}$ ) of section 2.2, but now exclusively *restricted to the injection domain*, that is, the compatibility equation is weakly imposed only for those elements belonging to the injection domain:

---

<sup>4</sup> Here we propose a modification in the methodology relatively to the previous works of the authors [1, 3] (in which the irreducible displacement formulation was used as underlying formulation). In section 3.4 we explain the motivation for this option.

$$\int_{\mathcal{B}^{(e)}} \boldsymbol{\mu}^{(e)} : (\dot{\boldsymbol{\varepsilon}}_{inj}^{(e)} - \nabla^s \dot{\mathbf{u}}^h(\mathbf{x})) d\mathcal{B} = 0, \quad \forall \boldsymbol{\mu}^{(e)}, \quad \forall \mathcal{B}^{(e)} \subset \mathcal{B}_{inj}(t). \quad (14)$$

In equation (14) the injected strain can be solved by repeating the process in equations (7)-(9):

$$\Rightarrow \dot{\boldsymbol{\varepsilon}}_{inj}^{(e)} = \dot{\boldsymbol{\varepsilon}}_{CSM}^{(e)} = \overline{\nabla^s \dot{\mathbf{u}}^h}^{(e)}, \quad \forall \mathcal{B}^{(e)} \subset \mathcal{B}_{inj}(t). \quad (15)$$

REMARK 3-1 The injection kinematics proposed in equation (15) is equivalent to the kinematics of the unstable mixed formulation in equation (8). The key difference is that (15) is just used in those elements belonging to the injection domain. We would like to remark that, using this injection concept, *no stabilization is needed* for the injected elements, since the use of the mixed stabilized formulation, of equation (12), in the larger part of the domain, prevents hourglass displacement modes to propagate at the structural level (rather than at the element level by stabilization).

REMARK 3-2 The CSM injection proposed in (15) still cannot resolve the discontinuity inside the finite element without stress locking (for general situations), but it provides a slight increase of flexibility in those finite elements that are good “candidates” to develop discontinuities, thus establishing a transitory stage to the Discontinuous-Displacement Mode (DDM) injection that will be presented at section 3.2.2.

### 3.2.2 Discontinuous-Displacement Mode (DDM) injection

The *discontinuous-displacement mode injection* consists of enriching the element kinematics with the strong discontinuity kinematics (summarized at Box 2) such that the mechanical behavior of the crack can be perfectly captured inside the finite element without spurious stress transfer to the neighboring elements (stress locking phenomena).

Strong discontinuity kinematics:

$$\dot{\boldsymbol{\varepsilon}} = \underbrace{\nabla^s \dot{\mathbf{u}} - \nabla \varphi \otimes \dot{\mathbf{u}}^s}_{\hat{\boldsymbol{\varepsilon}} \text{ (regular)}} + \delta_S \mathbf{n} \otimes \dot{\mathbf{u}}^s, \quad (16)$$

$S$  - Discontinuity surface,  
 $\mathbf{n}$  - Unit vector orthogonal to  $S$  (pointing to  $B^+$ ),  
 $\dot{\mathbf{u}}$  - Smooth part of the displacement field,  
 $\dot{\mathbf{u}}^s$  - Strong discontinuity jump ( $\dot{\mathbf{u}}^s = \dot{\mathbf{u}}|_{\mathbf{x} \in (\partial B^+ \cap S)} - \dot{\mathbf{u}}|_{\mathbf{x} \in (\partial B^- \cap S)}$ ),  
 $\delta_S$  - Dirac distribution shifted to  $S$ ,  
 $\varphi(\mathbf{x})$  - Continuous *indicator* function fulfilling:  $\varphi(\mathbf{x}) = \begin{cases} 0 & \forall \mathbf{x} \in \mathcal{B} \setminus \mathcal{B}_M^- \\ 1 & \forall \mathbf{x} \in \mathcal{B} \setminus \mathcal{B}_M^+ \end{cases}$ .

Box 2 Summary of the strong discontinuity kinematics (see [58]).

Inspired in the strong discontinuity kinematics in equation (16), the following element-wise constant discontinuous-displacement mode is proposed as the summation of a regular constant strain  $\dot{\bar{\varepsilon}}^{(e)}$  and a singular part  $\delta_{\mathcal{S}}^{k,(e)}(\dot{\mathbf{u}}^{(e)} \otimes \mathbf{n}^{(e)})^S$ <sup>5</sup>:

$$\dot{\varepsilon}_{inj}^{(e)} = \dot{\varepsilon}_{DDM}^{(e)} = \dot{\bar{\varepsilon}}^{(e)} + \delta_{\mathcal{S}}^{k,(e)}(\dot{\mathbf{u}}^{(e)} \otimes \mathbf{n}^{(e)})^S, \quad \forall \mathcal{B}^{(e)} \in \mathcal{B}_{inj}(t). \quad (17)$$

Equation (17) brings two new independent unknowns,  $\dot{\bar{\varepsilon}}^{(e)}$  and  $\dot{\mathbf{u}}^{(e)}$ , to the mechanical problem. Following the same process than in section 3.2.1, the two-field  $(\mathbf{u} / \varepsilon)$  mixed formulation of section 3 can be extended to a three-field  $(\hat{\mathbf{u}} / \bar{\varepsilon} / \mathbf{u})$  formulation which requires therefore, two additional equations. One comes from imposing weakly the equality between the regular part of the strong discontinuity kinematics,  $\dot{\bar{\varepsilon}}^{(e)}$ , in equation (16) and the regular constant strain,  $\dot{\bar{\varepsilon}}^{(e)}$ , in (17):

$$\int_{\mathcal{B}^{(e)}} \boldsymbol{\mu}^{(e)} : [\dot{\bar{\varepsilon}}^{(e)} - \underbrace{(\nabla^S \hat{\mathbf{u}}^h - (\nabla \varphi^h \otimes \dot{\mathbf{u}}^{(e)})^S)}_{\dot{\bar{\varepsilon}}^{(e)}}] d\mathcal{B} = 0, \quad \forall \mathcal{B}^{(e)} \in \mathcal{B}_{inj}, \quad \forall \boldsymbol{\mu}^{(e)}. \quad (18)$$

The constant strain  $\dot{\bar{\varepsilon}}^{(e)}$  can be condensed out at the element level as it was done for the CSM injection (repeating the process in equations (7)-(9)):

$$\Rightarrow \quad \dot{\bar{\varepsilon}}^{(e)} = \overline{\nabla^S \hat{\mathbf{u}}^h}^{(e)} - \overline{(\nabla \varphi^h \otimes \dot{\mathbf{u}}^{(e)})^S}^{(e)}, \quad \forall \mathcal{B}^{(e)} \in \mathcal{B}_{inj}(t). \quad (19)$$

And by substituting in equation (17), the injected strain field reads<sup>6</sup>:

$$\dot{\varepsilon}_{inj}^{(e)} = \dot{\varepsilon}_{DDM}^{(e)} = \overline{\nabla^S \hat{\mathbf{u}}^h}^{(e)} - \overline{(\nabla \varphi^h \otimes \dot{\mathbf{u}}^{(e)})^S}^{(e)} + \delta_{\mathcal{S}}^{k,(e)}(\dot{\mathbf{u}}^{(e)} \otimes \mathbf{n}^{(e)})^S, \quad \forall \mathcal{B}^{(e)} \in \mathcal{B}_{inj}(t). \quad (20)$$

### 3.3 Injection domains

After defining the strain modes to be injected, the subsequent questions to be posed are *where* and *when* these strain modes should be injected in order to effectively improve the performance of the finite elements for capturing strain localization. The answer to these questions is given by selecting proper injection domains. In the context of material failure modeling it is intuitively reasonable that the proposed strain modes should be injected in that part of the body where the fracture is being processed. By this reason the definition of the injection domains  $\mathcal{B}_{inj}(t)$  is grounded on consistent mechanical criteria, such as the *discontinuous bifurcation analysis* that qualifies a stress/strain state as compatible with the onset of a discontinuous displacement field. Two conditions are required to be fulfilled at the finite element barycenter  $\mathbf{x}_C^{(e)}$  to be considered part of the *injection domain*,  $\mathcal{B}_{inj}(t)$ :

---

<sup>5</sup>  $\delta_{\mathcal{S}}^{k,(e)}$  stands for the  $k$ -regularized Dirac distribution inside the element  $(e)$  (see [1]).

<sup>6</sup> After condensing the field  $\dot{\bar{\varepsilon}}^{(e)}$  at the element level, the finite element formulation simplifies in a two field formulation  $(\hat{\mathbf{u}} / \mathbf{u})$ . To solve the displacement jump,  $\mathbf{u}$ , traction continuity is imposed at the discontinuity surface  $([\dot{\boldsymbol{\sigma}}_{\mathcal{S}}^{+, (e)} \cdot \mathbf{n}^{(e)}]_{\mathcal{S}^{(e)}} = \mathbf{0})$ , as it is usually done in the Continuum Strong Discontinuity Approach (CSDA) (see [58]).

$$\mathcal{B}_{inj}(t) := \left\{ \bigcup_e \mathcal{B}^{(e)} ; \underbrace{t \geq t_B(\mathbf{x}_C^{(e)})}_1 ; \underbrace{\dot{\alpha}(\mathbf{x}_C^{(e)}, t) > 0}_2 \right\}. \quad (21)$$

Conditions in equation (21) can be described as:

- 1- The discontinuous bifurcation condition has been fulfilled in a previous time ( $t \geq t_B(\mathbf{x}_C^{(e)})$ ) where  $t$  stands for the actual time and  $t_B$  is the bifurcation time.
- 2- The element is in *in-loading* regime at the current time ( $\dot{\alpha}(\mathbf{x}_C^{(e)}, t) > 0$ )<sup>7</sup> since unloading elements cannot localize.

The *injection domain*,  $\mathcal{B}_{inj}$ , is that part of the domain where several strain mode injections can be performed (it has common conditions for all possible injections). In preceding sections two strain modes were proposed: the CSM and the DDM. Therefore two sub-sets of  $\mathcal{B}_{inj}$  ( $\mathcal{B}_{loc}$  and  $\mathcal{B}_{dis}$ ) where these strain modes are respectively injected must be defined, such that:  $\mathcal{B}_{inj}(t) = \mathcal{B}_{loc}(t) \cup \mathcal{B}_{dis}(t)$  and  $\mathcal{B}_{loc}(t) \cap \mathcal{B}_{dis}(t) = \emptyset$

### 3.3.1 The discontinuity injection domain

The *discontinuity injection domain*  $\mathcal{B}_{dis}(t) \subset \mathcal{B}_{inj}(t)$ , in which the discontinuous displacement mode (DDM) is injected, is the set of elements that have bifurcated and, in addition, are effectively developing a strain localization process<sup>8</sup>. The defining conditions, for a finite element to be part of the discontinuity domain, are three:

$$\mathcal{B}_{dis}(t) := \left\{ \bigcup_e \underbrace{\mathcal{B}^{(e)} \in \mathcal{B}_{inj}(t)}_1 ; \underbrace{q(\mathbf{x}_C^{(e)}, t) \leq q_{dis}(\mathbf{x}_C^{(e)})}_2 ; \underbrace{\mathcal{B}^{(e)} \cap \Gamma_t \neq \emptyset}_3 \right\}. \quad (22)$$

- 1- The element belongs to the injection domain, thus fulfilling conditions in (21).
- 2- The element has achieved a “sufficient degree of softening”<sup>9</sup>. This condition is implemented by defining a threshold in terms of the stress-like internal variable,  $q_{dis}(\mathbf{x}_C^{(e)})$ . If the actual value of the stress-like internal variable,  $q(\mathbf{x}_C^{(e)}, t)$ , evaluated at the barycenter of the finite element, is lower than the chosen threshold, the condition is considered fulfilled (see Figure 2).

---

<sup>7</sup>  $\dot{\alpha}(\mathbf{x}_C^{(e)}, t)$  stands for the strain-like internal variable, which is always positive for loading processes. Therefore loading is associated to increase of this variable  $\dot{\alpha} > 0$ .

<sup>8</sup> Notice that not all the bifurcated elements develop cracks; some of the elements that initially bifurcated unload elastically in subsequent time steps.

<sup>9</sup> This condition has the aim to guaranty that the element not only has bifurcated but is effectively developing a consistent strain localization process.

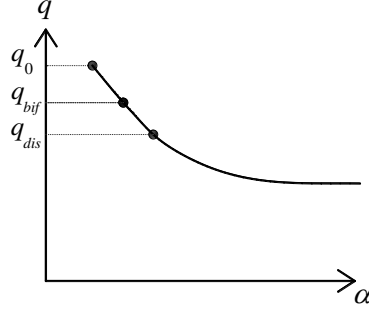


Figure 2 Thresholds in the evolution of the stress/strain-like internal variables ( $q/\alpha$ ), where  $q_0$  is the parameter characterizing the elastic strength and  $q_{bif}$  is the value taken by the variable at the bifurcation time.

Moreover, the threshold  $q_{dis}$ , can be consistently defined in terms of the value taken by the  $q$ -variable at the bifurcation time  $q_{bif}(\mathbf{x}_C^{(e)})$ :

$$q_{dis}(\mathbf{x}_C^{(e)}) = \bar{\gamma} q_{bif}(\mathbf{x}_C^{(e)}). \quad (23)$$

where  $\bar{\gamma}$  is a parameter defined by the user from the recommended interval: [0.9,1.0] (see REMARK 4-3).

- 3- The element is crossed by the discontinuity path  $\Gamma_t$ . In order to inject the DDM effectively, the discontinuity path should be identified little in advance. In the context of the strain injection techniques this is obtained by the Crack-Path Field technique described in Section 4.

### 3.3.2 The localization domain

This domain, where the constant strain mode is injected, includes all the in-loading bifurcated elements (belonging therefore to the injection domain, equation (21)) which do not verify, yet, the conditions for belonging to the discontinuity domain (equation (22)), *i.e.*:

$$\mathcal{B}_{loc}(t) = \mathcal{B}_{inj}(t) \setminus \mathcal{B}_{dis}(t). \quad (24)$$

Typically, this set of elements evolves very quickly during the loading process. In fact, part of the elements that initially bifurcate, tend to unload elastically in subsequent stages leaving, therefore, the injection domain, while others, crossed by the discontinuity, remain developing strain localization until verifying conditions in (22). At that moment those elements become part of the discontinuity injection domain,  $\mathcal{B}_{dis}$  (see Figure 3 and Figure 4 where two typical strain injection-loading processes are depicted).

## 3.4 Summary and motivation

In previous works of the authors, the strain-injection techniques were used in combination with a standard displacement-based finite element formulation whereas in the present work, we propose a modification consisting of using, as underlying formulation, the mixed stabilized mixed formulation. The reasons for this option are mainly related to the brittleness of the fracture process in large structures, as is the case of concrete dams, since, due to smaller size of the fracture process zone in front of the overall structure size, the fracture type approaches a brittle fracture process [11-15].

In the previous works the strain injection techniques were applied to a set of quasi-brittle fracture academic benchmarks and, for that case, yielding or damage occur in a diffuse manner in the neighborhood of the crack tip. In the context of the strain injection techniques, this was translated into a set of elements evolving in the front of the crack tip, being injected by a constant strain mode, which was then regarded as an “enhancement bulb”, (see Figure 3) improving the flexibility and propagation capabilities of the finite elements.

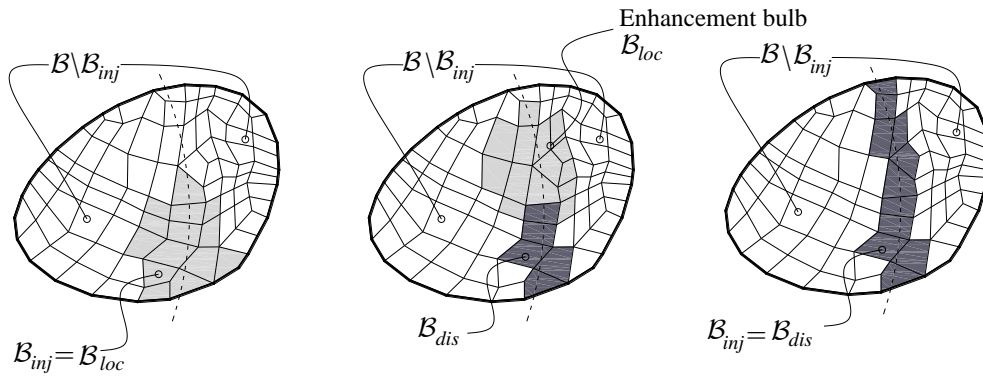


Figure 3 Evolution of the injection domains for three typical stages of loading in quasi-brittle fracture.

Instead, when modeling fracture propagation in concrete dams, due to the brittle behavior, the fracture process zone is much smaller<sup>10</sup>, and the enhancement bulb reduces, almost, to the elements crossed by the discontinuity (see Figure 3 and Figure 4 for an illustration).

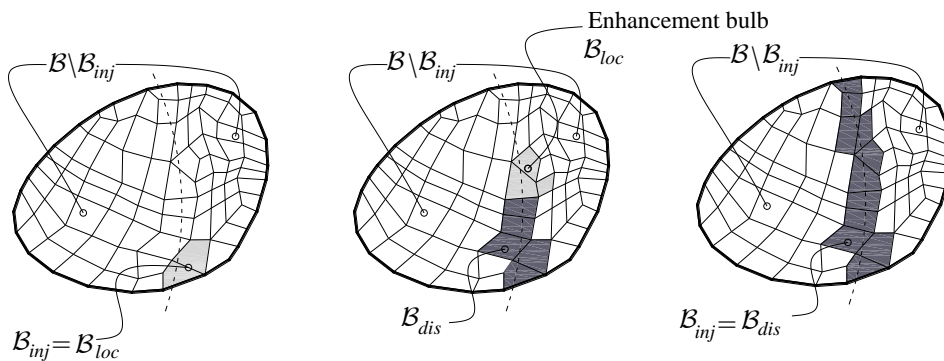


Figure 4 Evolution of the injection domains for three typical stages of loading in brittle fracture.

The principal inconvenient of this issue is that the enhancement bulb is too small (very few elements are injected with the more flexible constant kinematics) to avoid mesh alignment dependence. The choice for using the mixed stabilized formulation allow us to overcome this issue without drawbacks and with the advantage of constructing a more general methodology that can be used for modeling crack propagation for both large and small size structures.

With the definition of the strain modes and the respective injection domains in hand, equation (13) can be specified as follows:

<sup>10</sup> Hence a very fine mesh would be required in the fracture process zone.

$$\begin{aligned}
& \underbrace{\sum_{\forall \mathcal{B}^{(e)} \subset \mathcal{B} \setminus \mathcal{B}_{inj}} \int_{\mathcal{B}^{(e)}} \nabla^s \boldsymbol{\eta}^h : \dot{\boldsymbol{\sigma}}^{(e)}(\mathbf{x}) d\mathcal{B}}_{\text{Mixed stabilized formulation in } \mathcal{B} \setminus \mathcal{B}_{inj}} + \underbrace{\sum_{\forall \mathcal{B}^{(e)} \subset \mathcal{B}_{loc}(t)} \int_{\mathcal{B}^{(e)}} \nabla^s \boldsymbol{\eta}^h : \dot{\boldsymbol{\Sigma}}(\dot{\boldsymbol{\epsilon}}_{CSM}^{(e)}) d\mathcal{B}}_{\text{CSM injection in } \mathcal{B}_{loc}} \\
& + \underbrace{\sum_{\forall \mathcal{B}^{(e)} \subset \mathcal{B}_{dis}(t)} \int_{\mathcal{B}^{(e)}} \nabla^s \boldsymbol{\eta}^h : \dot{\boldsymbol{\Sigma}}(\dot{\boldsymbol{\epsilon}}_{DDM}^{(e)}) d\mathcal{B}}_{\text{DDM injection in } \mathcal{B}_{dis}} = +\dot{W}^{ext}(\boldsymbol{\eta}, \dot{\mathbf{b}}, \dot{\mathbf{t}}^*), \quad \forall \boldsymbol{\eta}^h.
\end{aligned} \tag{25}$$

where the strain modes,  $\dot{\boldsymbol{\epsilon}}_{CSM}^{(e)}$  and  $\dot{\boldsymbol{\epsilon}}_{DDM}^{(e)}$ , are defined by expression (15) and (20), respectively, and the stabilized stresses,  $\dot{\boldsymbol{\sigma}}^{(e)}$ , by expression (12).

REMARK 3-3 The mixed stabilized formulation in the first term of equation (25) brings extra flexibility to the proposed methodology, enhancing the propagation capabilities of the finite elements. Then, the injections proposed in section 3.2 allow resolving the discontinuity inside the finite element without spurious stress transfer. The final result is a mesh independent methodology ready for modeling the failure of real-life large concrete structures like concrete dams.

REMARK 3-4 The formulation proposed here is very general in the sense that it can be used for modeling strain localization for both large and small size structures. Moreover it can deal also with the locking effects arising from constitutive models that do not exhibit plastic change of volume, as is the case of  $J_2$  plasticity model (see [1]).

REMARK 3-5 The strain injection procedures proposed in this work, crucially rely on the incremental character of the injected strains, this allowing the smooth evolution, along time, of the corresponding strains and stresses, consistently with the evolutionary character of the injection domains. That is the reason for the mechanical problem of Box 1 to be stated in rate form.

## 4 Crack path field technique

Finite element formulations, either displacement-based or mixed ones, considering non-linear constitutive models equipped with strain softening (local, nonlocal, *etc.*), are widely used for studying fracture, which is represented by strain concentration in narrow bands. The crack path-field technique, proposed in [1-3], has the goal of determining the position of a strong discontinuity,  $\Gamma$ , represented by a diffuse strain localization field obtained from one of these methods.

### 4.1 One-dimension-problem: Motivation

The motivation for the numerical technique is very intuitive and can be illustrated, for the one-dimensional continuum case, as shown in Figure 5. The basic idea is to understand the diffuse localized field  $\alpha$  as a regularization of a strong discontinuity whose *position*,  $\Gamma$ , *can be assumed at the maximum value of the continuum function*  $\alpha$ . In practice, the maximum of the *continuum function*  $\alpha$ , can be determined by the zero value of its derivative.

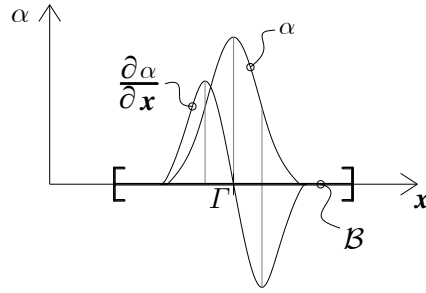


Figure 5 Hypothetical distribution of a localizing strain-like internal variable and its derivative in a continuum one dimensional problem.

Considering now the discrete case (as obtained from a linear finite element interpolation) shown in Figure 6, where the variable  $\alpha$  is available at the sampling points, the strategy to determine the position of  $\Gamma$  is the following:

- 1- Compute  $\psi^h$  as a smooth continuous approximation of the localized variable  $\alpha^h$
- 2- Compute the directional derivative  $\frac{\partial \psi^h}{\partial x}$
- 3- Compute  $\mu^h$  as a smooth continuous approximation of the derivative  $\frac{\partial \psi^h}{\partial x}$
- 4- Determine the crack-path position,  $\Gamma$ , as the zero level set of  $\mu^h$

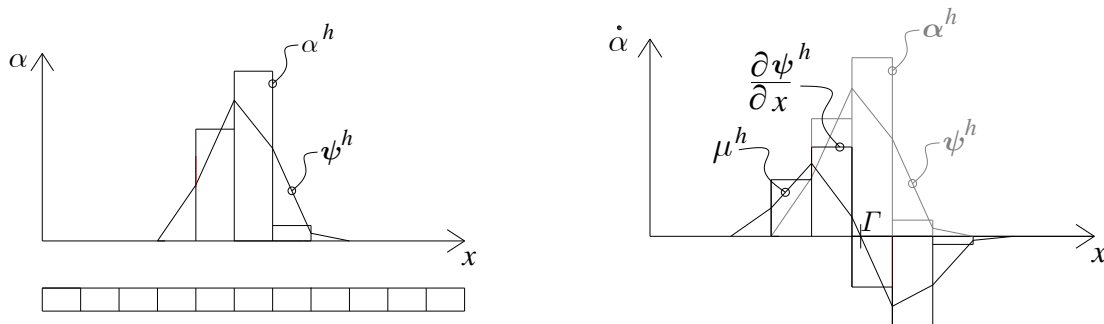


Figure 6 Discretized one dimensional problem: a) Hypothetical distribution of a localizing strain-like internal variable; b) Hypothetical distribution of the derivative of a localizing strain-like internal variable.

REMARK 4-1 In the previous procedure, function  $\mu^h$  is obtained by a double smoothing procedure of the localized variable  $\alpha^h$  (Figure 7). Then the crack-path position  $\Gamma$  is determined as the zero level set of  $\mu^h$ .

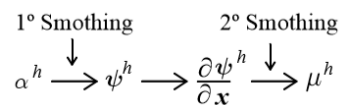


Figure 7 Double smoothing process



Notice that in some points outside the localization zone the function  $\mu^h$  takes also null values (see Figure 6 b)) not corresponding to maxima of  $\psi^h$ , but instead, corresponding to the trivial case:

$$\alpha^h = 0 \rightarrow \psi^h = 0 \rightarrow \frac{\partial \psi^h}{\partial x} = 0 \rightarrow \mu^h = 0 \quad (26)$$

In practice, these not interesting zones of  $\mu^h = 0$  (not corresponding to  $\Gamma$ ) do not introduce any additional trouble since they are located in elements outside the non-linear zone where no strains localize and so are easily identified by the numerical procedure as non-interesting zeros.

## 4.2 Crack path problem

The ideas presented in the previous can be formalized in the crack-path-field problem summarized in Box 3.

- 1- Compute  $\psi^h$  as a smooth continuous approximation of the localizing variable  $\alpha^h$ :

$$\int_{\mathcal{B}^h} \bar{\psi}^h (\psi_t^h - \alpha^h(\mathbf{x}, t)) d\mathcal{B} = 0, \quad \forall \bar{\psi}^h.$$

- 2- Compute the derivative in the direction orthogonal to the discontinuity,  $\mathbf{n}$ :

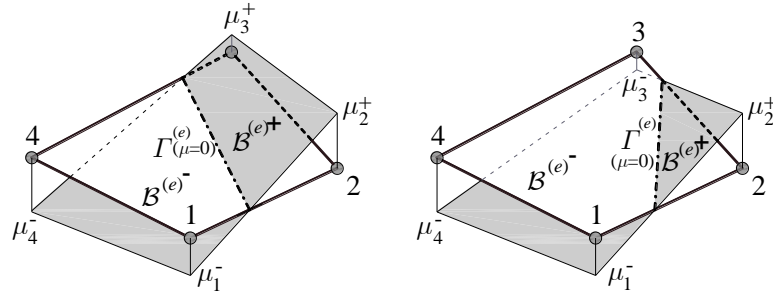
$$\frac{\partial \psi_t^h}{\partial n} = \nabla \psi_t^h \cdot \mathbf{n}.$$

- 3- Compute  $\mu^h$  as a smooth continuous approximation of the directional derivative:

$$\int_{\mathcal{B}^h} \bar{\mu}^h (\mu_t^h - \nabla \psi_t^h \cdot \mathbf{n}) d\mathcal{B} = 0, \quad \forall \bar{\mu}^h.$$

- 4- Determine the crack-path position,  $\Gamma_t$ , as the zero level set of  $\mu_t^h$  in an elemental basis:

$$\Gamma_t^h := \mathbf{x} \in \mathcal{B}^h; \mu_t^h(\mathbf{x}) = 0 \rightarrow \text{zero level set of } \mu_t^h(\mathbf{x}).$$



Box 3 Summary of the Crack-path-field problem [1-3].

REMARK 4-2 In [1] a more formal and rigorous presentation of the technique, and its implementation details, can be consulted by the interested readers. More information can also be found in [2, 3].

REMARK 4-3 In order to perform the discontinuous mode injection two typical questions arise: a) *Which elements have to be injected?* b) *For the injected elements, how does the discontinuity cross the finite element?* In the context of the strong discontinuity approach, this information is generally obtained by resorting to global tracking algorithms [59]. Here, the strain-injection technique is used in combination with the described crack-path field

technique. A crucial issue of the method is that the crack-path-field has to be sufficiently well captured at the time of the DDM injection. In order to achieve this goal a delay in the DDM injection has to be imposed. This delay is controlled by the parameter  $\bar{\gamma}$  in equation (23). From the author's experience,  $\bar{\gamma} = 0.95$  provides a good balance between the (little) error produced by delaying the injection and the need of having reliable information from the crack-path field technique prior to that injection.

## 5 Representative numerical simulations

In this section two representative numerical simulations of gravity concrete dams were studied. The first example consists of a concrete dam scale model (of a 96-m-high gravity dam) where experimental measurements obtained in a laboratory are available for comparison [4]. The second example consists of a full-scale concrete gravity dam (Koyna dam), which has been used as a case study by numerous researchers [14, 17, 26, 27, 45, 51].

For the material behavior modeling, a *plasticity-based* Rankine constitutive model equipped with strain softening (properly regularized such that dissipation matches the material fracture energy) is used. It is not the first time that a Rankine model, implemented within the framework of plasticity theory, is used for material failure modeling of concrete structures. In [60] a Rankine plasticity model was used for modeling mode-I crack propagation in some academic benchmarks.

In this work, for the integration of the constitutive equation, an implicit-explicit (IMPL-EX) scheme [61, 62] is used, which translates in a high increase of robustness of the numerical procedure when compared to fully implicit integration schemes, in which lack of robustness issues are well known in the context of computational failure modeling [63].

### 5.1 A gravity dam model

In [4] Carpinteri et al. experimental tests of scale-down models of a gravity dam have been reported. The models have a horizontal notch on the upstream side and the experimental test was driven by controlling the crack mouth opening at that notch. Figure 8 illustrates the experiment setup, including the model dimensions, the position of the notch and the equivalent hydraulic loads. The finite element mesh and the mechanical properties used in the numerical model are also shown in the figure.

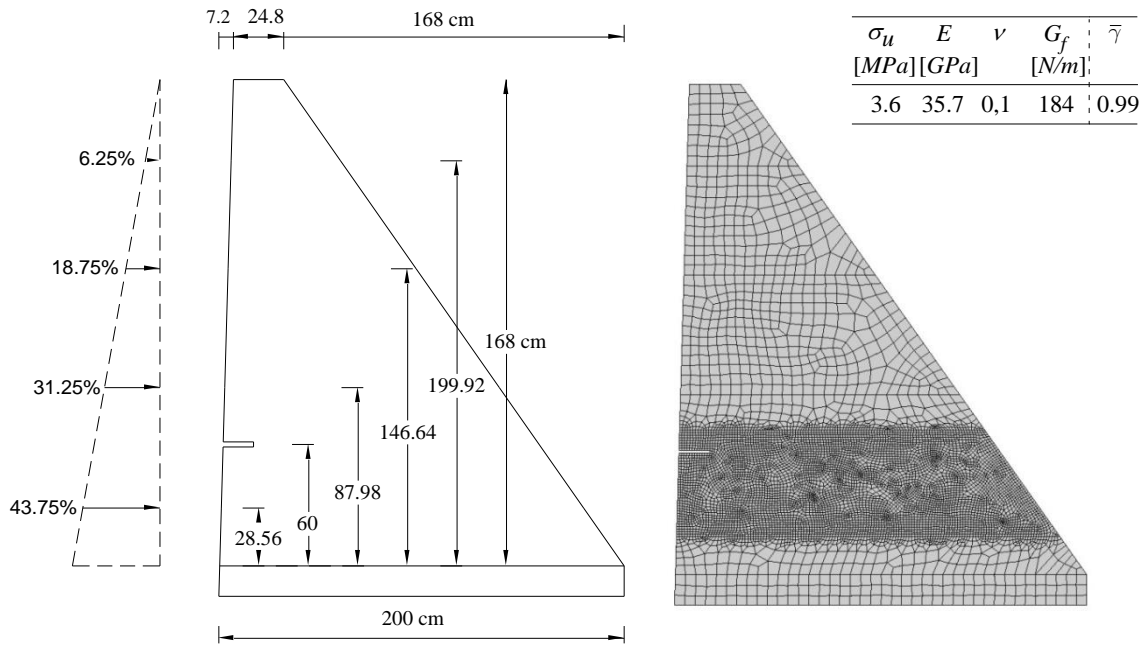


Figure 8 Dam model, finite element mesh and mechanical properties used in the numerical model, being  $\sigma_u$  the ultimate tensile strength,  $E$  the Young's modulus,  $\nu$  the Poisson's ratio and  $G_f$  the fracture energy.

In the numerical simulations, the loading process was performed by applying, in a first stage, the self-weight loads and, in a second stage, the hydraulic loads. The second stage is carried out through a step by step Newton-Raphson scheme in which the crack mouth displacement at the notch is controlled by using arc-length techniques. All the computations were performed under plane strain conditions.

In Figure 9 quantitative responses for three different options are depicted in terms of the force–CMOD (Crack-Mouth-Opening Displacement) curves. The “strain injection” curve was obtained by using the strain injection techniques described in this work, while the “experimental” and “cohesive model curves” were obtained by Carpinteri et al, being the former experimentally measured and the later numerically computed by using a cohesive crack model supported in an automatic remeshing processes, at each crack growth step, so that the crack lies in the finite element mesh sides.

Figure 9 shows an excellent agreement between both numerical solutions. The obvious advantage of the strain injection technique is that no remeshing process is needed. Relatively to the comparison with the experimental solution the peak load is well captured although the post peak response curve is much stiffer in the experimental test. Reasons for this may relay on some issues of the experimental set-up that are missed in the numerical model.

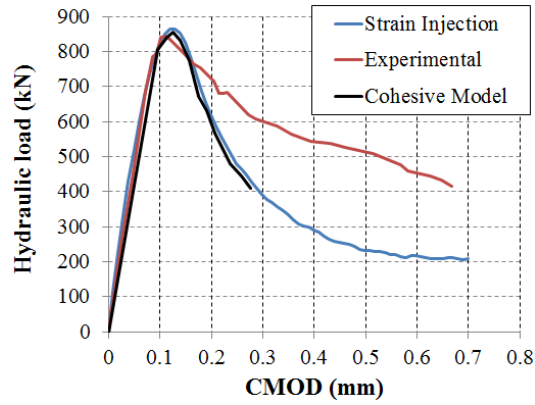


Figure 9 Force displacement curves: hydraulic load versus Crack Mouth Opening Displacement (CMOD).

In terms of crack propagation patterns, Figure 10 shows a good agreement between the experimental and the numerical results obtained with the strain injection techniques. Finally, Figure 11 shows the deformed configuration and the crack path at the final stage of the loading process.

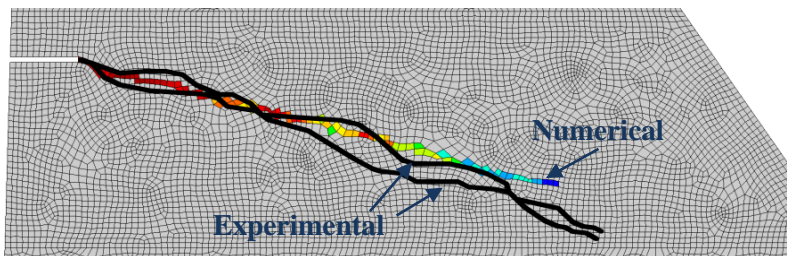


Figure 10 Crack trajectories. The numerical solution crack pattern is plotted in terms of the equivalent plastic strain. The experimental trajectories have been added to the figure through the black lines corresponding to both sides of the experimental 3d model.

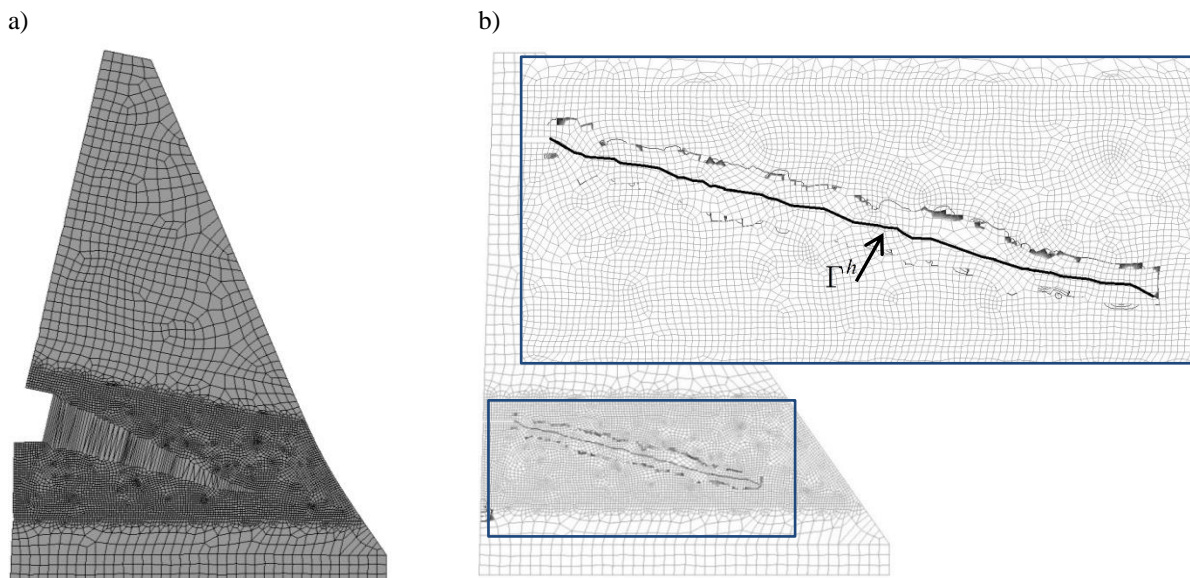


Figure 11 a) Deformed configuration; b) Crack path  $\Gamma^h(\mu^h = 0)$ <sup>11</sup>.

Results obtained by the strain injection techniques at the final step of the computations.

<sup>11</sup> The grey regions in Figure 11 b), at some distance of the crack path, correspond to regions where  $\mu^h$  approach zero outside the zones where the strain are localizing, do not having any physical meaning neither any influence in the computations (see REMARK 4-1).

### 5.1.1 Mesh dependency analysis

When modeling material failure, mesh dependence is a critical issue since different meshes can deliver different results, in terms either of the crack trajectory or in terms of the dissipated energy. Mesh dependence phenomena is well documented in the literature and displays essentially two types of undesirable behavior that are summarized in Section 1: Mesh bias dependence and stress locking effects.

In order to assess if the results obtained by using the injection techniques are mesh independent, comparative analysis were carried out by using two different fine meshes: one structured and another unstructured (Figure 12). Additionally, the obtained results are also compared with the ones coming from standard displacement-based (irreducible) formulations, which are known to suffer from mesh dependence. Finally the results obtained with the strain injection techniques by using an unstructured coarse mesh are also presented.

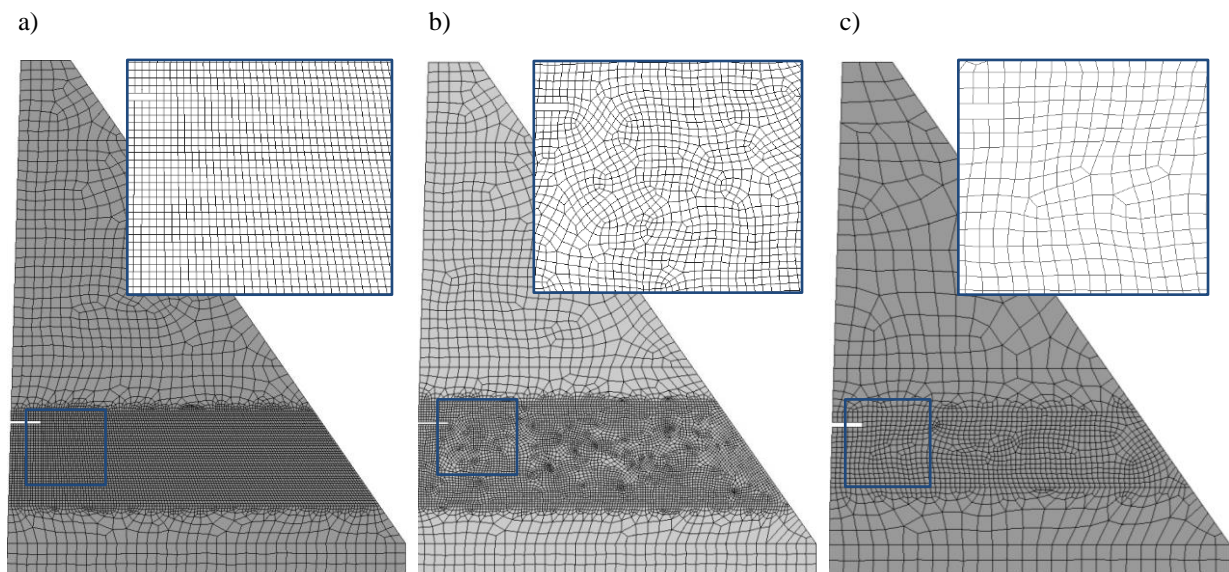


Figure 12 Finite element meshes; a) structured fine mesh; b) unstructured fine mesh; c) unstructured coarse mesh

Figure 13 compares results obtained with the two finite element formulations (strain injection techniques and irreducible formulation) for both fine meshes in Figure 12. Since the Rankine constitutive model is the same for both formulations, the differences in Figure 13 can be exclusively attributed to the performance of the finite element formulation.

In fact, the results obtained with the irreducible formulation show a considerably stiffer behavior in terms of the post-peak response that can be related to spurious extra energy dissipation due to stress locking defects. This issue has also consequences in the peak load which is miss-predicted for the irreducible formulation when using the unstructured mesh. Although, for this specific example, the differences in terms of the peak load are not too large (less than 10 %), we would like to remark that the results obtained with the irreducible formulation are not on the safety side.

Relatively to the results obtained by using the strain injection techniques and the coarse unstructured mesh, it can be observed that the peak load is slightly miss-predicted but the post-peak behavior is very well captured, this indicating that similar amount of energy is being dissipated for both (fine and course) meshes, this clearly proving the mesh-size objectivity of the obtained results.

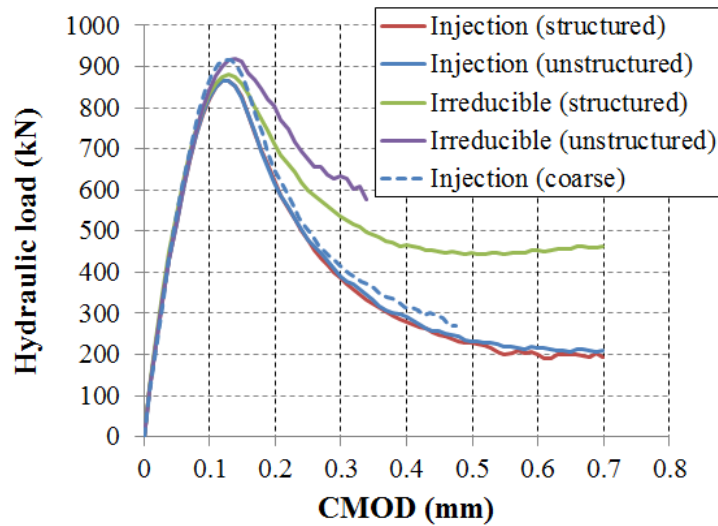


Figure 13 Finite element meshes; a) structured mesh; b) unstructured mesh

It is also remarkable that results obtained by strain injection technique, for both fine meshes, are almost the same, which is a strong indicator of mesh independence. This can be noticed either by the overlapping curves in Figure 13 or by the near coincident crack trajectories in Figure 14.

For the coarse unstructured mesh, although the results in Figure 14 show some differences in terms of the crack trajectories (which are corrected with mesh refinement), this doesn't translate, as mentioned before, into relevant differences in the quantitative structural response (see Figure 13).

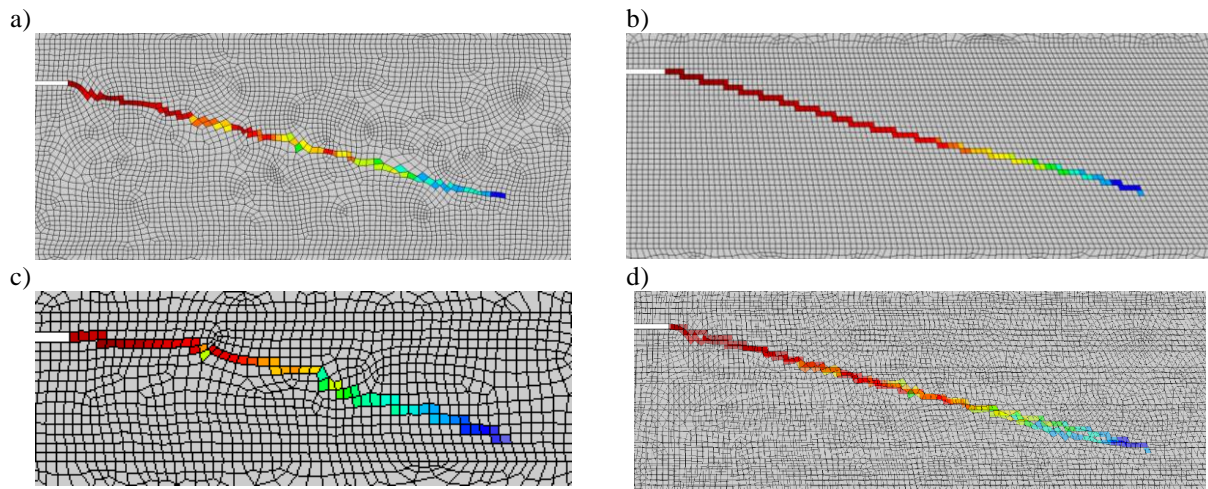


Figure 14 Results obtained by using the strain injection techniques. Crack patterns plotted in terms of the equivalent plastic strain; a) Unstructured fine mesh; b) Structured fine mesh; c) Unstructured coarse mesh; d) overlap of results obtained with both fine meshes.

Relative to the results obtained by the irreducible formulation, Figure 15 shows different results in terms of the crack patterns. This issue is related to the mesh bias influence, since the crack pattern obtained for the structured mesh seems to be clearly influenced by horizontal mesh direction.

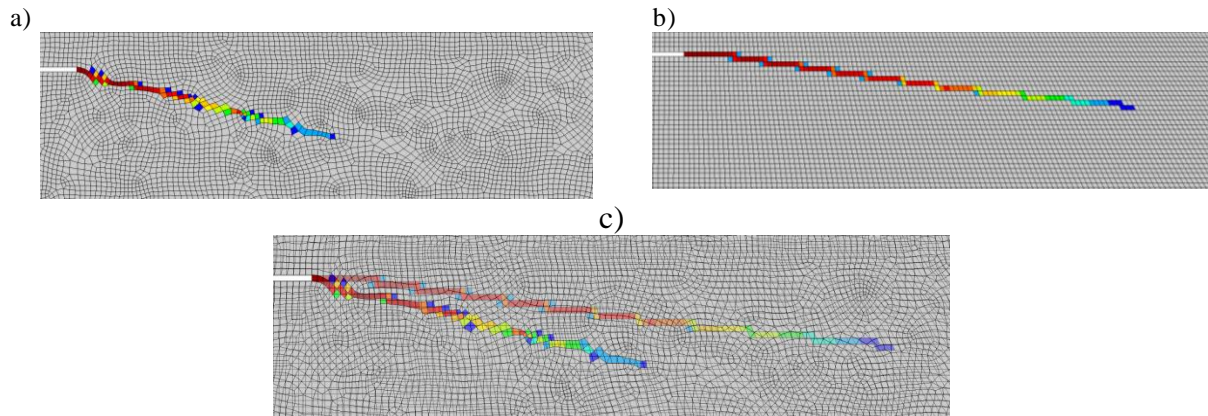


Figure 15 Results obtained by using the irreducible formulation. Crack patterns plotted in terms of the equivalent plastic strain; a) Unstructured fine mesh; b) Structured fine mesh; c) overlap of results obtained with both meshes.

## 5.2 Full size concrete gravity dam

The Koyna Dam in India, whose geometry is depicted in Figure 16, is an example of a full-scale concrete gravity dam that can be used for testing new modeling techniques. The crack propagation throughout the dam body, under quasi-static conditions, caused by an hypothetical overflow, was first studied by Gioia [14] by using linear elastic fracture mechanics. The authors found that a crack developing from point B in Figure 16, is the most critical in terms of the ultimate structural resistance and, for this reason, an initial imperfection is assigned to that location.

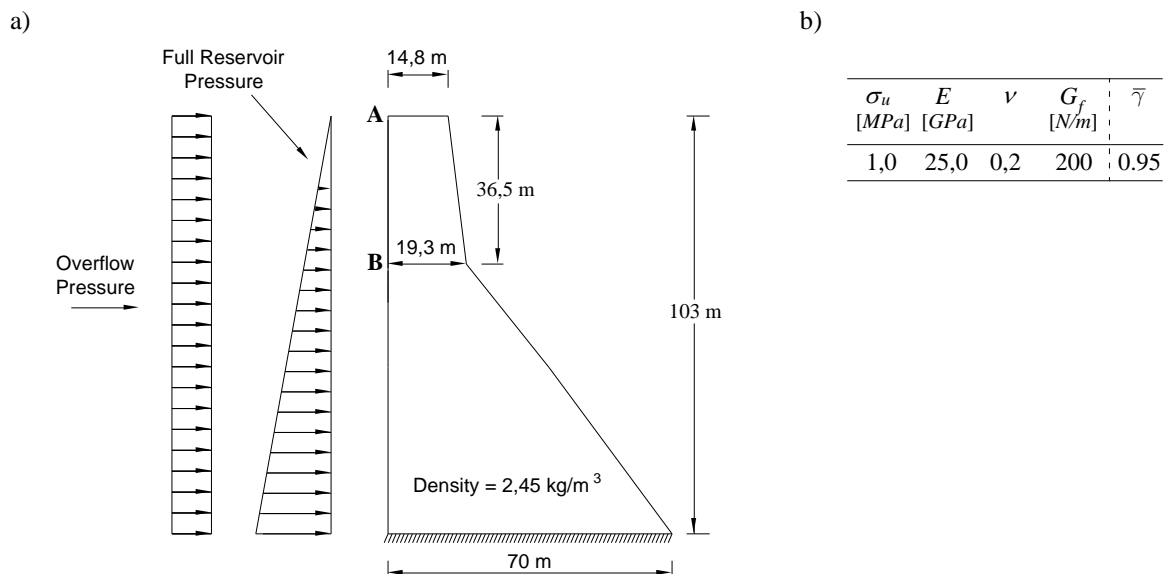


Figure 16 Koyna Dam. a) geometrical description; b) material properties, being  $\sigma_u$  the ultimate tensile strength,  $E$  the Young's modulus,  $\nu$  the Poisson's ratio and  $G_f$  the fracture energy.

During the numerical simulations, the dam initially undergoes its self-weight and the full reservoir hydrostatic pressure, and then, is subjected to a step by step constant pressure increase due to overflow. The loading corresponding to the overflow is indirectly applied by using arc-length techniques in which the crack mouth opening displacement at point B is controlled. All the computations were performed under plane strain conditions.

For assessing the mesh influence in the obtained results two distinct finite element meshes, structured and unstructured, are used (Figure 17).

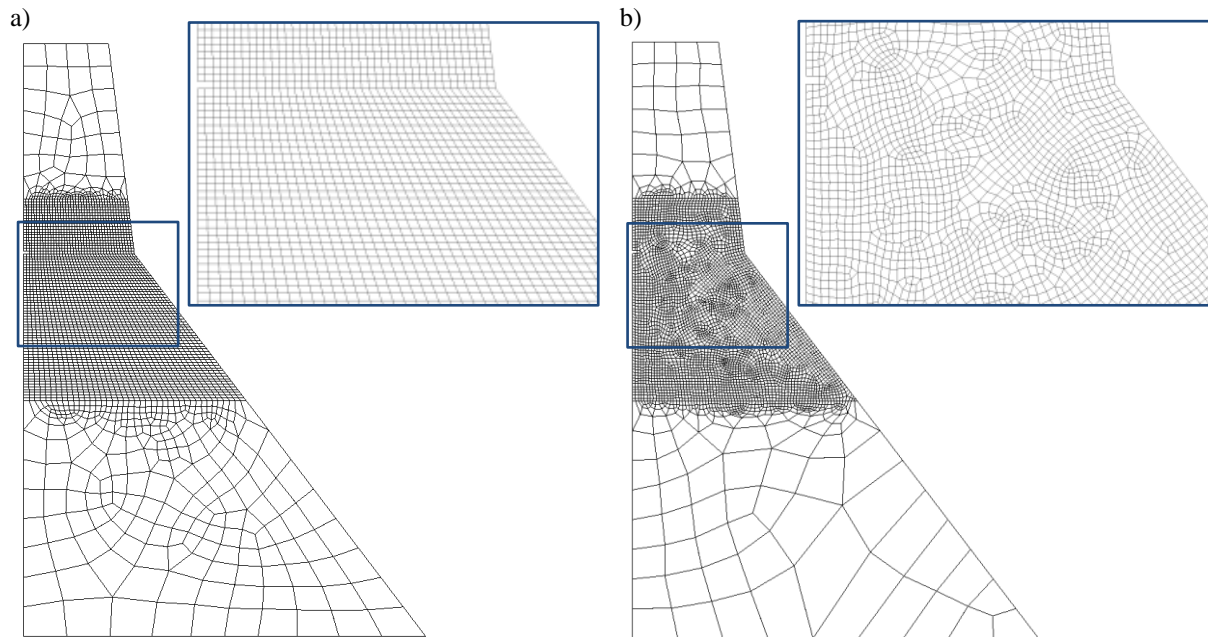


Figure 17 Finite element meshes; a) structured mesh; b) unstructured mesh.

The analysis of the results are performed in two stages:

- 1- First, the results obtained with the injection techniques and both finite element meshes (of Figure 17) are compared.
- 2- Second, the results obtained with the injection techniques are compared with results obtained by using an irreducible finite element formulation. Since in both cases, the constitutive model is the same, the eventual enhanced behavior reflects, exclusively, improvements related to the finite element formulation. Comparison with other authors' results is also performed at this stage.

### 5.2.1 Results obtained with the strain injection techniques

Figure 18 illustrates the dam structural response, due to the overflow, in terms of the displacement measured at the top (point A of Figure 16).

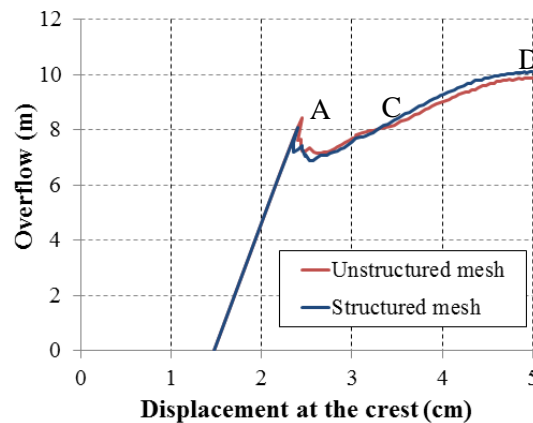


Figure 18. Comparison of results obtained using the strain injection techniques for two different meshes (Figure 17). Structural resistance to reservoir overflow.



The curves of Figure 18 display minimal differences which is a strong indication of very similar structural behavior. For both meshes, point A is a limit point, from where the crack progresses without increasing the load (“snap-through”) until point C. After this point, of unstable physical crack propagation, the crack still grows but requiring load increase. Figure 19 and Figure 20 show the crack propagation evolution at three different stages of the computations (see the points in Figure 18), for the unstructured mesh.

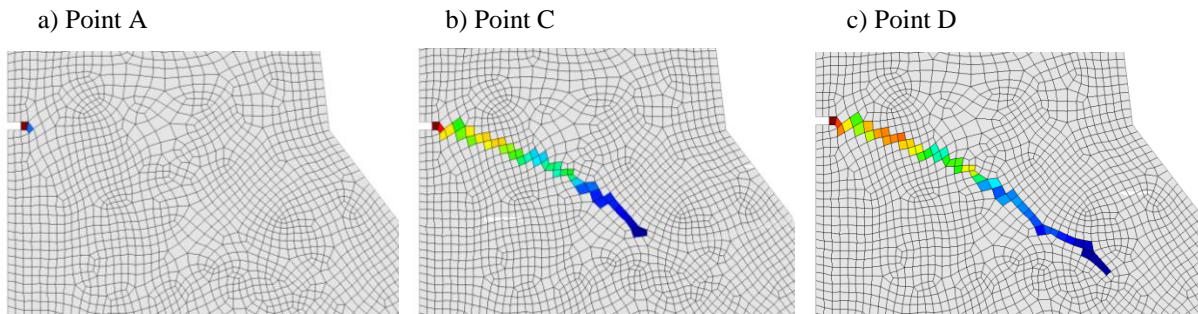


Figure 19 Results obtained with the strain injection techniques for the unstructured mesh. Crack patterns, plotted in terms of the equivalent plastic strain, for the three points represented in Figure 18.

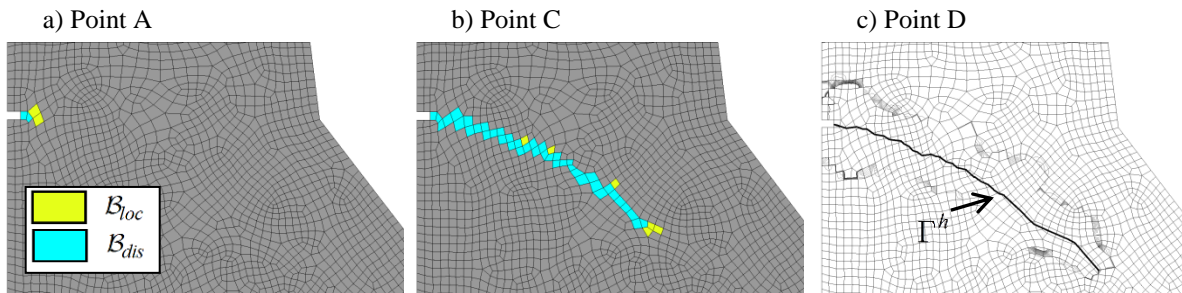


Figure 20 Results obtained with the strain injection techniques for the unstructured mesh. Crack propagation and injection domains; a) and b) Evolution of the injection domain at point A and C of Figure 18; c) crack path,  $\Gamma^h(\mu^h = 0)$ <sup>12</sup>, at Point D.

Figure 21 compares the results obtained using both meshes in terms of the crack propagation. This comparison clearly displays that both solutions are very similar in terms of the crack pattern (see Figure 21 c)) which indicates that the results are independent of the mesh alignment. Figure 22 shows the deformed configurations for both finite element meshes.

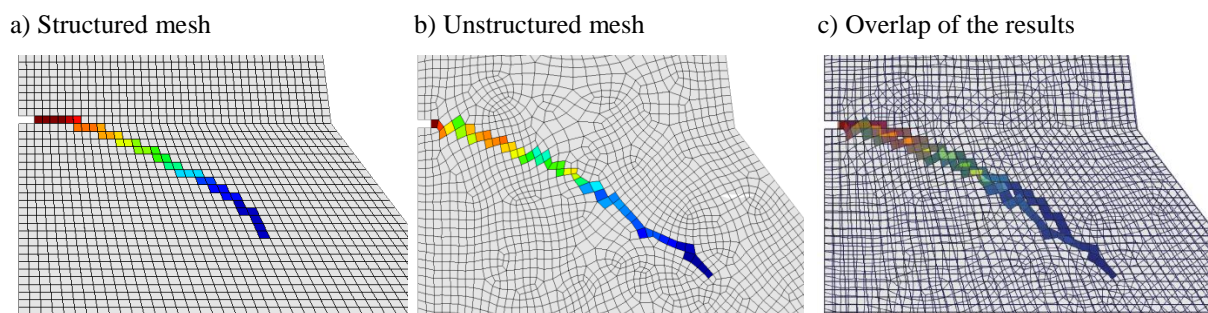


Figure 21 Crack patterns plotted in terms of the equivalent plastic strain; a) Structured mesh; b) Unstructured

<sup>12</sup> The grey regions in Figure 20 c), at some distance of the crack path, correspond to regions where  $\mu^h$  approach zero outside the zones where the strain are localizing, do not having any physical meaning neither any influence in the computations (see REMARK 4-1).

mesh; c) Overlap of both solutions in the same plot.  
Results obtained using the strain injection techniques.

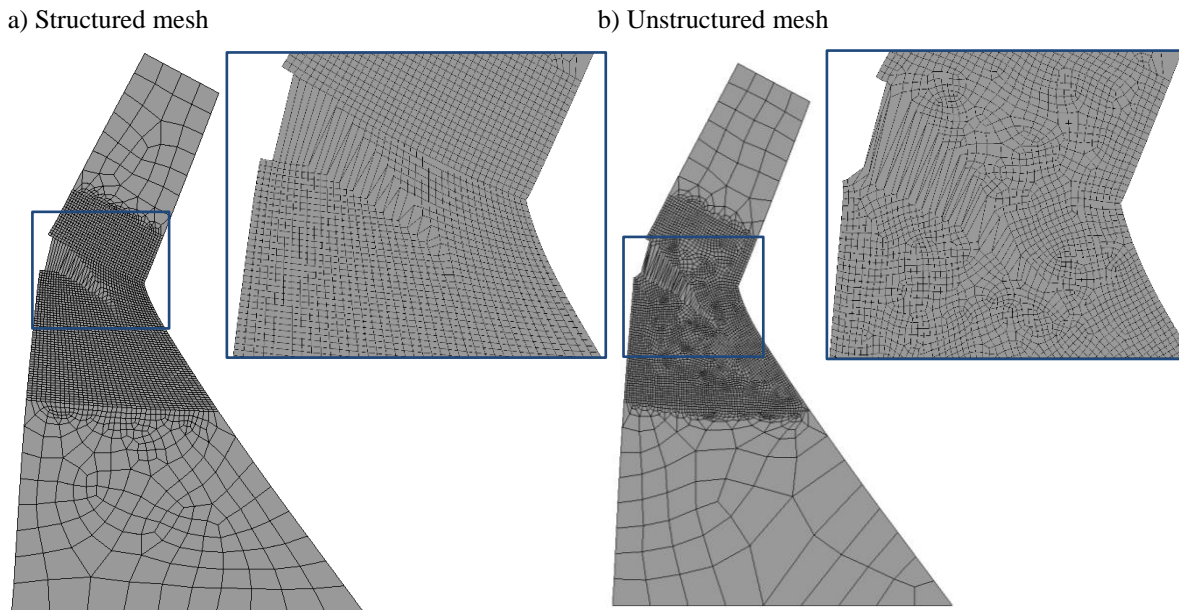


Figure 22 Deformed configurations.  
Results obtained using the strain injection techniques.

### 5.2.2 Comparisons with the classic displacement-based finite element formulation

In Figure 23, results obtained with the proposed techniques are compared with those obtained with the displacement-based irreducible formulation and by Gioia [14] using Linear Elastic Fracture Mechanics (LEFM).

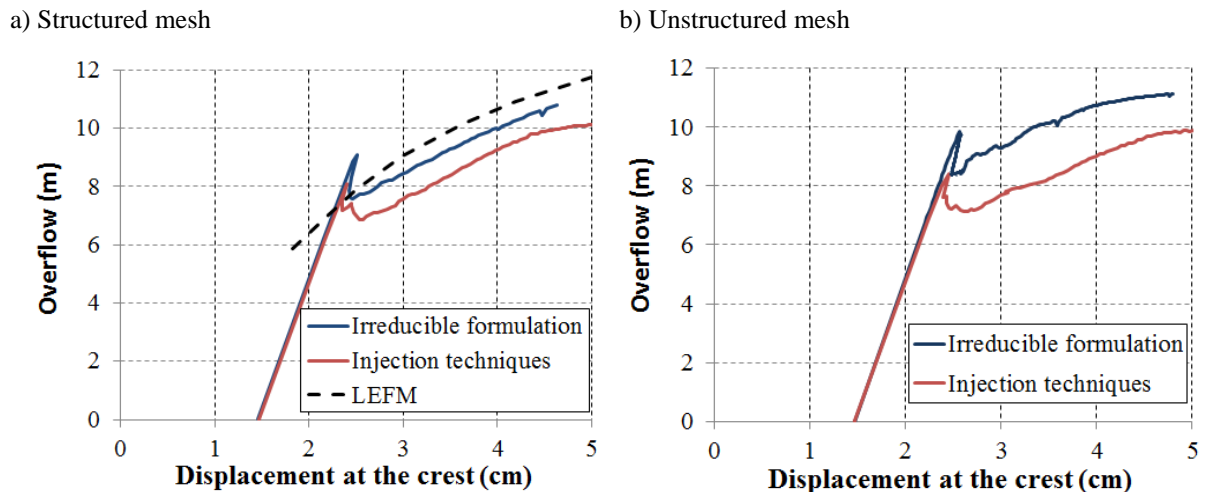


Figure 23 Structural resistance to reservoir overflow. Comparison of results obtained using the strain injection techniques and the irreducible formulation for both meshes of Figure 17: a) Structured mesh; b) Unstructured mesh.

There it can be checked that, due to stress locking effects, the classical formulations overestimate the ultimate structural load carrying capacity. This mesh dependent behavior is further noticeable for the unstructured mesh, which is consistent with the fact that stress locking effects are, normally, more

severe for this kind of meshes. In Figure 23 it is also included the result obtained by Gioia (LEFM), using a structured mesh under plane strain conditions<sup>13</sup>.

Spurious stress locking effects can also be identified by the plot of the equivalent plastic deformation in Figure 24. This figure shows that, for the results obtained with the classical formulation, the non-linear effects spread spuriously, by several elements in the direction orthogonal to the crack. Instead, for the results obtained with the strain injection techniques the plastic effects are highly concentrated in a one-element-width localization band, this indicating that no spurious stresses are being transferred by the open crack.

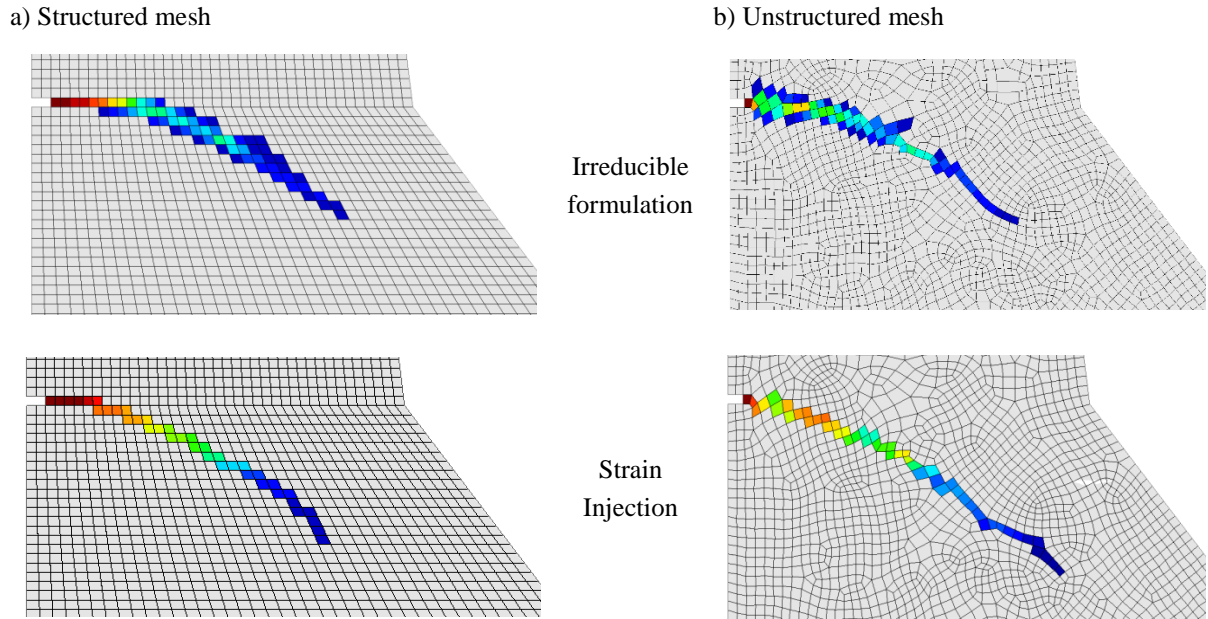


Figure 24 Crack patterns plotted in terms of the equivalent plastic strain. Comparison of results obtained using the strain injection techniques and the irreducible formulation for both meshes of Figure 17.

These results clearly display the advantages of the strain injection techniques in front of the classical irreducible formulations. In particular, they show that stress locking effects are effectively minimized.

## 6 Conclusions

In this work, the potential of the recently proposed strain injection techniques, so far with applications limited to some academic benchmarks, has been explored for studying crack propagation in concrete gravity dams.

The obtained results clearly show the improvements obtained by using the proposed methodology in terms of mesh independence, either avoiding mesh bias or stress locking effects. This spurious undesirable behavior can lead to unrealistic failure mechanisms or to the overestimation of the ultimate structural load carrying capacity. In the Konya simulation, for instance, the displacement

---

<sup>13</sup> Other authors have studied crack propagation in this dam (*cf.* [17, 27, 51]) in plane stress conditions. Although the obtained results are not too different, a rigorous comparison cannot be performed due to the different choice of the plane analysis assumptions, and for this reason, comparisons with those results have been skipped in this work.

based classical formulation delivers results overestimating the structural resistance in about 20 %, which is not on the safety side.

The new methodology has several advantages that the authors would like to remark:

- Mesh independence of the results.
- Low computational cost – the explored approach captures the crack inside the finite element, which means that coarse meshes can be used when compared with the finer meshes required by other methodologies (nonlocal [31, 32, 64], phase field [33, 47], *etc.*) that use several elements across the band for modeling the crack. Moreover, all the additional degrees of freedom (related to the enhanced strain modes) are condensed out at the element level. The final result is a methodology that keeps the computational cost at the level of the standard displacement-based finite element formulations.
- Nonintrusive numerical implementation in existing finite element codes – The strain-injection technique in combination with the crack-path-field technique avoids the code invasive global crack tracking algorithms, usually used in association with other intra-elemental approaches (E-FEM [58] or X-FEM [65]), with no apparent cost in terms of robustness. This issue is a strong advantage, since the implementation tasks, in a non-linear finite element code, affect, essentially, the element level.
- Constitutive model generality – the method affects exclusively the finite element formulation, this meaning that, in principle, any continuum constitutive model equipped with strain softening can be used within the formulation.

Due to these important properties, that address the main issues of material failure modeling (mesh independence, computational cost, robustness), the strain injection techniques render a methodology particularly efficient for modeling tensile crack propagation in concrete dams. Moreover, the results obtained in this paper show that the method is ready for being used in practice, allowing improved estimation of the structural safety factor and helping in the security control of those gravity concrete dams which might be particularly vulnerable to crack propagation.

The ongoing extension of the presented methodology to 3D cases will open the application field to large arch dams.

## **ACKNOWLEDGMENTS**

Ivo Dias gratefully acknowledges the financial support from Laboratório Nacional de Engenharia Civil (LNEC), through a postdoctoral research grant (CoMatFail project).

The research leading to these results has received funding from the European Research Council under the European Union's Seventh Framework Programme (FP/2007-2013) / ERC Grant Agreement n. 320815 (ERC Advanced Grant Project "Advanced tools for computational design of engineering materials" COMP-DES-MAT).

Oriol Lloberas-Valls gratefully acknowledges the funding received from the Spanish Ministry of Economy and Competitiveness through the "Juan de la Cierva" Postdoctoral Junior Grant: JCI-2012-13782 and the *National Research Plan 2014: MAT2014-60919-R*.

## REFERENCES

- [1]. Oliver, J., Dias, I.F., and Huespe, A.E., Crack-path field and strain-injection techniques in computational modeling of propagating material failure. *Computer Methods in Applied Mechanics and Engineering*, 2014. 274(0): p. 289-348.
- [2]. Dias, I.F., *Crack Path Field and Strain Injection Techniques in Numerical Modeling of Propagating Material Failure*. 2012, Ph.D. Thesis. Universitat Politècnica de Catalunya: (BarcelonaTech/UPC), Barcelona, Spain.
- [3]. Dias, I.F., Oliver, J., and Huespe, A.E., *Strain Injection Techniques in Numerical Modeling of Propagating Material Failure*, in *Monograph CIMNE N°-134*. 2012, International Center for Numerical Methods in Engineering: Barcelona. <http://www.cimne.com/compdesmat/cvdata/cntr1/dtos/img/mdia/Downloads/M134.pdf>.
- [4]. Carpintieri, A., Valente, S.V., Ferrara, G., and Imperato, A.L. *Experimental and Numerical Fracture Modelling of a Gravity Dam*. in *Fracture Mechanics of Concrete Structures*. 1992: Elsevier Appl. Sci.
- [5]. Anderson, C., Mohorovic, C., Mogck, L., Cohen, B., and Scott, G., *Concrete Dams : Case Histories of Failures and Nonfailures with Back Calculations*. 1998: U.S. Department of Interior, Bureau of Reclamation, Dam Safety Office.
- [6]. Charles, J.A., Tedd, P., and Warren, A., *Lessons from Historical Dam Incidents: Technical Summary*. 2011: Environment Agency.
- [7]. CSED, *Safety of Existing Dams: Evaluation and Improvement*. 1983: The National Academies Press.
- [8]. ICOLD, *Lessons from dam incidents*. Complete ed ed. 1974, Paris: ICOLD.
- [9]. Strom, R.W., Cunningham, G., and Safety, I.C.o.D., *Training Aids for Dam Safety: Evaluation of Concrete Dam Stability*. 1990: U.S. Government Printing Office.
- [10]. ICOLD, *Monitoring of dams and their foundations. State of the art. Bulletin number 68*. 1989, Paris: ICOLD.
- [11]. Saouma, V.E., Ayari, M.L., and Boggs, H. *Fracture Mechanics of Concrete Gravity Dams*. in *SEM/RILEM International Conference on Fracture of Concrete Rock*. 1987. Houston, Texas,.
- [12]. Chappell, J., Ingraffea, F., and R., C.A., *A fracture mechanics investigation of the cracking of Fontana Dam*. Report 81-7. 1981, Ithaca, New York: Cornell University, Department of Structural Engineering, School of Civil and Environmental Engineering.
- [13]. Linsbauer, H.N. *Fracture mechanics models for characterizing crack behaviour of gravity dams*. in *Proceedings of the 15th ICOLD*. 1985. Lausanne.
- [14]. Gioia, G., Bazant, Z.P., and Pohl, B.P., Is no-tension dam design always safe. *Dam Engineering*, 1992. 3: p. 23-34.
- [15]. Plizzari, G., LFM Applications to Concrete Gravity Dams. *Journal of Engineering Mechanics*, 1997. 123(8): p. 808-815.
- [16]. Brühwiler, E. and Wittmann, F.H., Failure of dam concrete subjected to seismic loading conditions. *Engineering Fracture Mechanics*, 1990. 35(1-3): p. 565-571.
- [17]. Bhattacharjee, S. and Léger, P., Application of NLFM Models to Predict Cracking in Concrete Gravity Dams. *Journal of Structural Engineering*, 1994. 120(4): p. 1255-1271.
- [18]. Hillerborg, A., Modeer, M., and Petersson, P.E., Analysis of crack formation and crack growth in concrete by means of fracture mechanics and finite elements. *Cement and concrete research*, 1976. 6(6): p. 773-782.
- [19]. Dugdale, D.S., Yielding of steel sheets containing slits. *Journal of the Mechanics and Physics of Solids*, 1960. 8(2): p. 100-104.
- [20]. Rots, J.G., *Computational Modeling of Concrete Fracture*. 1988, Delft University of Technology.
- [21]. Rashid, Y., Analysis of prestressed concrete pressure vessels. *Nuclear Engineering and Design* 1968. 7: p. 773-782.
- [22]. Oliver, J., Cervera, M., Oller, S., and Lubliner, J. *Isotropic damage models and smeared crack analysis of concrete*. in *Proc. SCI-C Computer Aided Analysis and Design of Concrete Structures*. 1990.

- [23]. Pietruszczak, S. and Mróz, Z., Finite element analysis of deformation of strain-softening materials. *International Journal for Numerical Methods in Engineering*, 1981. 17(3): p. 327-334.
- [24]. Barpi, F. and Valente, S., Numerical Simulation of Prenotched Gravity Dam Models. *Journal of Engineering Mechanics*, 2000. 126(6): p. 611-619.
- [25]. Shi, Z., Suzuki, M., and Nakano, M., Numerical Analysis of Multiple Discrete Cracks in Concrete Dams Using Extended Fictitious Crack Model. *Journal of Structural Engineering*, 2003. 129(3): p. 324-336.
- [26]. Cai, Q., Robbets, J.M., and Van Rensburg, B.W.J., Finite element fracture modeling of concrete gravity dams. *Journal of the South African Institution of Civil Engineering*, 2008. 50(1): p. 13-24.
- [27]. Ghrib, F. and Tinawi, R., Nonlinear Behavior of Concrete Dams Using Damage Mechanics. *Journal of Engineering Mechanics*, 1995. 121(4): p. 513-527.
- [28]. Xu, Q., Chen, J.-y., Li, J., and Xu, G., Coupled elasto-plasticity damage constitutive models for concrete. *Journal of Zhejiang University SCIENCE A*, 2013. 14(4): p. 256-267.
- [29]. Cervera, M., Oliver, J., and Faria, R., Seismic Evaluation of Concrete Dams Via Continuum Damage Models. *Earthquake Engineering & Structural Dynamics*, 1995. 24(9): p. 1225-1245.
- [30]. de Araújo, J. and Awruch, A.M., Cracking safety evaluation on gravity concrete dams during the construction phase. *Computers & Structures*, 1998. 66(1): p. 93-104.
- [31]. Pijaudier Cabot, G. and Bazant, Z., Nonlocal damage theory. *Journal Engineering Mechanics ASCE*, 1987. 113: p. 1512-1533.
- [32]. de Borst, R. and Mühlhaus, H.-B., Gradient-dependent plasticity: Formulation and algorithmic aspects. *International Journal for Numerical Methods in Engineering*, 1992. 35(3): p. 521-539.
- [33]. Miehe, C., Welschinger, F., and Hofacker, M., Thermodynamically consistent phase-field models of fracture: Variational principles and multi-field FE implementations. *International Journal for Numerical Methods in Engineering*, 2010. 83(10): p. 1273-1311.
- [34]. Oliver, J., Huespe, A., and Sanchez, P., A comparative study on finite elements for capturing strong discontinuities: E-FEM vs X-FEM. *Computer Methods in Applied Mechanics and Engineering*, 2006. 195(37-40): p. 4732-4752.
- [35]. Mosler, J. and Meschke, G., Embedded crack vs. smeared crack models: a comparison of elementwise discontinuous crack path approaches with emphasis on mesh bias. *Computer Methods in Applied Mechanics and Engineering*, 2004. 193(30-32): p. 3351-3375.
- [36]. Bažant, Z., Tabbara, M., Kazemi, M., and Pijaudier-Cabot, G., Random Particle Model for Fracture of Aggregate or Fiber Composites. *Journal of Engineering Mechanics*, 1990. 116(8): p. 1686-1705.
- [37]. Potyondy, D.O. and Cundall, P.A., A bonded-particle model for rock. *International Journal of Rock Mechanics and Mining Sciences*, 2004. 41(8): p. 1329-1364.
- [38]. Meguro, K. and Hakuno, M., Fracture analyses of concrete structures by the modified distinct element method. *Structural Engineering/Earthquake Engineering*, 1989. 6(2): p. 283-294.
- [39]. Azevedo, N.M., Lemos, J.V., and de Almeida, J.R., Influence of aggregate deformation and contact behaviour on discrete particle modelling of fracture of concrete. *Engineering Fracture Mechanics*, 2008. 75(6): p. 1569-1586.
- [40]. Herrmann, H.J. and Roux, S., *Modelization of fracture in disordered systems*, in *Statistical Models for the Fracture of Disordered Media*, S.R. H. J. Hemmann, Editor. 1990, North-Holland: Amsterdam. p. 159-188.
- [41]. Schlangen, E. and Garboczi, E.J., Fracture simulations of concrete using lattice models: Computational aspects. *Engineering Fracture Mechanics*, 1997. 57(2-3): p. 319-332.
- [42]. Kozicki, J. and Tejchman, J., 2D Lattice Model for Fracture in Brittle Materials. *Arch. Hydro-Engrg. Environ. Mech*, 2006. 53(2): p. 137-154.
- [43]. Saether, E., Yamakov, V., Phillips, D.R., and Glaessgen, E.H., *An Overview of the State of the Art in Atomistic and Multiscale Simulation of Fracture* NASA/TM-2009-215564, Editor. 2009.
- [44]. Gumbsch, P., An Atomistic Study of Brittle Fracture: Towards Explicit Failure Criteria from Atomistic Modelling. *J. Mater. Res.*, 1995. 10: p. 2897-2907.

- [45]. Jirásek, M. and Zimmermann, T., Rotating Crack Model with Transition to Scalar Damage. *Journal of Engineering Mechanics*, 1998. 124(3): p. 277-284.
- [46]. Oliver, J., Dias, I.F., and Huespe, A., *Strong discontinuities, mixed finite element formulations and localized strain injection, in fracture modeling of quasi-brittle materials*, in *Computational Modelling of Concrete Structures*. 2010, CRC Press. p. 381-389.
- [47]. Miehe, C., Hofacker, M., and Welschinger, F., A phase field model for rate-independent crack propagation: Robust algorithmic implementation based on operator splits. *Computer Methods in Applied Mechanics and Engineering*, 2010. 199(45–48): p. 2765-2778.
- [48]. Cervera, M., Chiumenti, M., and Codina, R., Mesh objective modeling of cracks using continuous linear strain and displacement interpolations. *International Journal for Numerical Methods in Engineering*, 2011. 87(10): p. 962-987.
- [49]. Linder, C. and Raina, A., A strong discontinuity approach on multiple levels to model solids at failure. *Computer Methods in Applied Mechanics and Engineering*, 2013. 253: p. 558-583.
- [50]. Chen, L., Rabczuk, T., Bordas, S.P.A., Liu, G.R., Zeng, K.Y., and Kerfriden, P., Extended finite element method with edge-based strain smoothing (ESm-XFEM) for linear elastic crack growth. *Computer Methods in Applied Mechanics and Engineering*, 2012. 209-212: p. 250-265.
- [51]. Roth, S.-N., Léger, P., and Soulaïmani, A., A combined XFEM–damage mechanics approach for concrete crack propagation. *Computer Methods in Applied Mechanics and Engineering*, 2015. 283: p. 923-955.
- [52]. Simó, J. and Ju, J., Strain and stress based continuum damage models. I. Formulation. *International Journal of Solid and Structures*, 1987. 23: p. 821-840.
- [53]. Malkus, D.S. and Hughes, T.J.R., Mixed finite element methods - reduced and selective integration techniques: a unification of concepts. *Comp. Meth. Appl. Mech. Eng.*, 1978. 15: p. 63-81.
- [54]. Kosloff, D. and Frazier, G.A., Treatment of hourglass patterns in low order finite element codes. *International Journal for Numerical and Analytical Methods in Geomechanics*, 1978. 2(1): p. 57-72.
- [55]. Belytschko, T. and Bachrach, W.E., Efficient implementation of quadrilaterals with high coarse-mesh accuracy. *Comput. Methods Appl. Mech. Eng.*, 1986. 54(3): p. 279-301.
- [56]. Bochev, P. and Gunzburger, M., An Absolutely Stable Pressure-Poisson Stabilized Finite Element Method for the Stokes Equations. *SIAM J. Numer. Anal.*, 2004. 42(3): p. 1189-1207.
- [57]. Dohrmann, C.R. and Bochev, P.B., A stabilized finite element method for the Stokes problem based on polynomial pressure projections. *International Journal for Numerical Methods in Fluids*, 2004. 46(2): p. 183-201.
- [58]. Oliver, J. and Huespe, A.E., Continuum approach to material failure in strong discontinuity settings. *Computer Methods in Applied Mechanics and Engineering*, 2004. 193(30-32): p. 3195-3220.
- [59]. Oliver, J., Huespe, A.E., Samaniego, E., and Chaves, E.W.V. *On Strategies for Tracking Strong Discontinuities in Computational Failure Mechanics*. in *Fifth World Congress on Computational Mechanics (WCCM V)*. 2002. Vienna University of Technology, Austria.
- [60]. Feenstra, P. and de Borst, R., Constitutive model for reinforced concrete. *Journal of Engineering Mechanics – ASCE*, 1995. 121(5): p. 587-595.
- [61]. Oliver, J., Huespe, A., Blanco, S., and Linero, D., Stability and robustness issues in numerical modeling of material failure with the strong discontinuity approach. *Computer Methods in Applied Mechanics and Engineering*, 2006. 195(52): p. 7093-7114.
- [62]. Oliver, J., Huespe, A., and Cante, J., An implicit/explicit integration scheme to increase computability of non-linear material and contact/friction problems. *Computer Methods in Applied Mechanics and Engineering*, 2008. 197(21-24): p. 1865-1889.
- [63]. Crisfield, M.A., *Non-Linear Finite Element Analysis of Solids and Structures: Advanced Topics, 1st edition* 1997, New York, NY, USA John Wiley & Sons, Inc. 508.
- [64]. Iordache, M.-M. and Willam, K., Localized failure analysis in elastoplastic Cosserat continua. *Comput. Methods Appl. Mech. Engrg.*, 1998(151): p. 559-586.
- [65]. Belytschko, T., Moes, N., Usui, S., and Parimi, C., Arbitrary discontinuities in finite elements. *International Journal for Numerical Methods in Engineering*, 2001. 50(4): p. 993-1013.